Passive arching in rubberised sand backfills

Hamidreza Khatami,

Corresponding author, E-mail: hamidreza.khatami@adelaide.edu.au

School of Civil, Environmental, and Mining Engineering, The University of Adelaide, Adelaide, South Australia 5000, Australia

An Deng,

E-mail: an.deng@adelaide.edu.au

School of Civil, Environmental, and Mining Engineering, The University of Adelaide, Adelaide, South Australia 5000, Australia

Mark Jaksa

E-mail: mark.jaksa@adelaide.edu.au

School of Civil, Environmental, and Mining Engineering, The University of Adelaide, Adelaide, South Australia 5000, Australia

Abstract

The deformation and stress profiles of passive arching in a coarse sand and two rubberised sand backfills were investigated using a trapdoor apparatus. The trapdoor apparatus was instrumented with high-speed imaging equipment and a series of pressure sensors. The images of the deformation process in the backfills were analysed using the digital image correlation technique. The effect of a local surcharge on the deformation and stress profiles was also examined. It was observed that the rubber inclusions helped reduce the deformation of the backfills. Passive arching moduli and stress variations between the backfills examined are compared.

Keywords: Rubber–sand, arching effect, digital image correlation, deformation, trapdoor apparatus, dilation angle.

1. Introduction

It is estimated that approximately 48 million waste tyres are dumped annually in Australia (Tyrecycle, 2018). The large amount of waste tyres, and the increasingly stringent requirements of environmental protection legislation demand effective and sustainable management solutions. For example, the Environment Protection Authority (EPA) of South Australia no longer allows waste whole tyres to be disposed to landfill. Worldwide, the current principal waste tyre handling schemes include re-treading, energy recovery, civil engineering applications, and other miscellaneous applications, such as rubberised asphalt, agricultural fertilizers, art and crafts, furniture, and playgrounds. Civil engineering applications make a significant contribution to the sustainable use of waste tyres. In 2011, it was estimated that approximately 8% of recycled waste tyres were utilised in civil engineering applications (Rubber Manufacturers Association, 2013). Rubber-based geomaterials are one such example of a civil engineering application using recycled waste tyres and they are classified into two forms: shredded tyres as a substitute for natural aggregate, referred to as Tyre–Derived Aggregate (TDA); and recycled tyres mixed with natural sand, which are referred to as rubber–sand. Humphrey (1999) and Edil (2004) outlined the engineering characteristics of recycled tyres that can be exploited by civil and geotechnical engineers. These properties include light weight, thermal insulation, high permeability, low horizontal pressures, good damping properties, and low chemical leachate. The mechanical properties of these geomaterials for different applications, such as road construction and retaining walls, have been assessed by many researchers (e.g. Eldin and Senouchi, 1992; Humphrey and Sandford, 1993; Bosscher et al., 1997; Tweedie et al., 1998; Lee at al., 1999; Edinçliler et al., 2004; Shalaby and Khan, 2005; Yoon et al., 2006; Lee and Roh, 2007; Ahn and Cheng, 2014). Negligible impact on groundwater quality using waste rubber has also been reported by Eldin and Senouchi (1992) and Humphrey and Blumenthal

(2010). New guidelines to use TDA and rubber–sand mixtures as aggregate are provided in ASTM D6270 (ASTM, 2017) and ASTM D7760 (ASTM, 2018) standards.

While extensive data on the mechanical properties of rubber–sand mixtures are available in the literature, it seems that little is known about the arching behaviour of rubberised backfills. Arching influences the stress regime in a granular geomaterial, both in the vertical and horizontal directions due to induced differential displacements. Active arching occurs when the stresses decrease on the yielding part of the material assembly as a result of the mobilisation of shear resistance on the opposite direction to the induced displacement. Active arching has been examined in a number of studies (e.g. Terzaghi, 1936; Dewoolkar et al. 2007; Costa et al., 2009; Chevalier et al., 2012; Iglesia et al., 2013; van Eekelen, 2015). On the other hand, inclusion of structural elements, such as a fixed, single piles into a geomaterial, followed by movement of the surrounding geomaterial later in time, as a result of creep for example, results in a passive arching effect or increased loads on the structural element. This may in turn lead to serviceability issues or even structural failure. In addition, assessment of deformability of a geomaterial associated with a structure become more important than analysing the stresses because serviceability or failure of the structure, due to excessive settlement or deformation, may precede the failure of the geomaterial. Therefore, it is necessary to measure or predict the arching deformations and account for them in design. The range of allowable deformation depends on the project specifications and application. However, it is reported that the allowable strains in most common geotechnical projects such as foundations, retaining walls, and tunnels fall in the general range of 0.1%–1% without a severability issue (Mair, 1979). For embankments, for example, the typical movement due to self-weight is 0.1% of the height of the embankment (Look, 2007). Other examples of passive arching include pile groups, where a pile may experience both active and passive arching on different sides (Shelke and Patra, 2008; Yuan, et al., 2014), anti-sliding or

stabilisation piles inserted into soil slopes (Chen and Martin, 2002; Kahyaoğlu et al., 2012; He et al., 2015), swelling of soil around an underground structure (Aqoub et al., 2018), or even soil pressure sensors where over-registration of stress values indicate passive arching on the sensor (Talesnick, 2013).

Studies on passive arching, however, lag behind, perhaps because the active arching case is considered to be more common in practice. This current study therefore aims to address the deformation and stress response of a sand and two rubberised sand backfills subjected to passive arching. The effect of geomaterial type and local surcharge on deformation fields and stress response on the structure-geomaterial interface was studied. Shear band formation was a particular focus. The digital image correlation (DIC) technique was used to map the distribution of displacements and strains. A series of benchmark tests on the sand and rubberised sand backfills was performed using a replicate of Terzaghi's trapdoor apparatus (Terzaghi, 1936). During the arching process, the stresses were recorded using a number of stress cells and the deformations were measured using the DIC technique.

2. Materials and methods

Silica sand and rubber particles, both sourced from local suppliers, were used as the backfill. The rubber particles were produced from shredded recycled tyres with steel belts removed. Approximately 95% of the sand particles were in the range of 1.18–2.36 mm; and the rubber particles were between 5–13 mm in size. The other properties of Sand and Rubber–sand mixtures are provided in Table 1. The rubber–sand mixtures represent 10% or 30% rubber by weight calculated as follows:

$$Rubber\ content\ (\%) = \frac{mass\ of\ rubber}{mass\ of\ sand\ +\ mass\ of\ rubber} \times 100\% \quad (1)$$

Past studies (e.g. a comprehensive review by Edil, 2004) has shown that rubber inclusion up to 35% by weight is effective in improving shear strength parameters of sand. Further addition of rubber beyond this limit has resulted in a reverse effect. For this reason, 10% and 30% rubber concentrations were investigated in this research. The minimum and maximum dry density of the material samples were determined using the procedure described by the Australian Standard 1289.5.5.1 (Standards Australia, 1998). The values of the effective angle of internal friction (φ') were determined using direct shear tests specified by AS 1289.6.2.2 (Standards Australia, 1998). To accommodate for larger sizes, the portion of rubber particles greater than one fifth of the smallest dimension of the shear box, which measured 60 mm × 60 mm × 38 mm, was sieved out, as proposed by Head and Epps (2010). However, the rubber percentage was maintained at the levels of 10% and 30%. The effective friction angle data from the direct shear tests, rounded to the nearest 0.5°, are also presented in Table 1.

Table 1. Physical properties of the backfill materials

Material	Density range (kg/m^3)	Backfill density	Size range of 95% of particles (mm)	Median size D_{50} (mm)	φ'
Sand	1,486–1,709	1,657	1.18–2.36	1.75	45°
10% Rubber–sand	1,367–1,574	1,515	1.18–9.5	1.81	44.5°
30% Rubber–sand	1,270–1,433	1,387	1.18–11.5	2.02	51°

As shown in Table 1, with the addition of rubber to Sand, the density decreased considerably, as expected. In relation to the friction angle, rubber at low percentages (e.g. 10%) had a very modest effect on the shear strength. However, increasing the rubber content to 30% resulted in a significant rise of 6° in the effective friction angle. Therefore, rubberised

backfills possess the advantage of reduced weight and improved shear strength, when compared to the original base aggregate.

The DIC technique requires a random speckle pattern on the specimen surface. Therefore, prior to backfill preparation, a speckle pattern was artificially imparted to the sand particles by dying approximately 30% by weight of the particles with a matte black colour. Matte paints minimise the effect of spectral light reflection which would otherwise introduce inaccuracies in the image correlation results. A number of Sand and rubberised sand backfills were prepared in a trapdoor apparatus using the air pluviation technique. The geomaterials were poured in equal batches from appropriate heights to a relative density of 76.5% ± 2.5%; hence to a medium-dense consistency. The density of the backfills tested in the trapdoor apparatus are listed in Table 1. Efforts were made to place the materials evenly, aiming to eliminate segregation and minimise heterogeneity in the Rubber–sand backfills.

The trapdoor apparatus was a cuboid container with dimensions of 1 m by 1 m by 0.2 m, as shown in Fig. 1. The front face of the trapdoor was fabricated using a transparent acrylic sheet, thus enabling imaging. The trapdoor and the static sides were constructed from rigid timber. The trapdoor element was 160 mm wide and, in order to create passive arching of the backfill, was designed, with the aid of a hydraulic jack, to translate upwards at a speed of 3.2 mm/s, to maximum displacement of 20 mm. The displacement of the trapdoor was measured by a linear variable displacement transducer (LVDT) with a sampling rate of 16 Hz installed underneath. The backfills were poured to a total depth of 250 mm, thus replicating a shallow arching condition, where the ratio of backfill depth to trapdoor width is less than 2 (Costa et al., 2009). A concrete block, 160 mm × 200 mm × 230 mm in size, was placed centrally on the backfill surface to apply a 5 kPa surcharge.

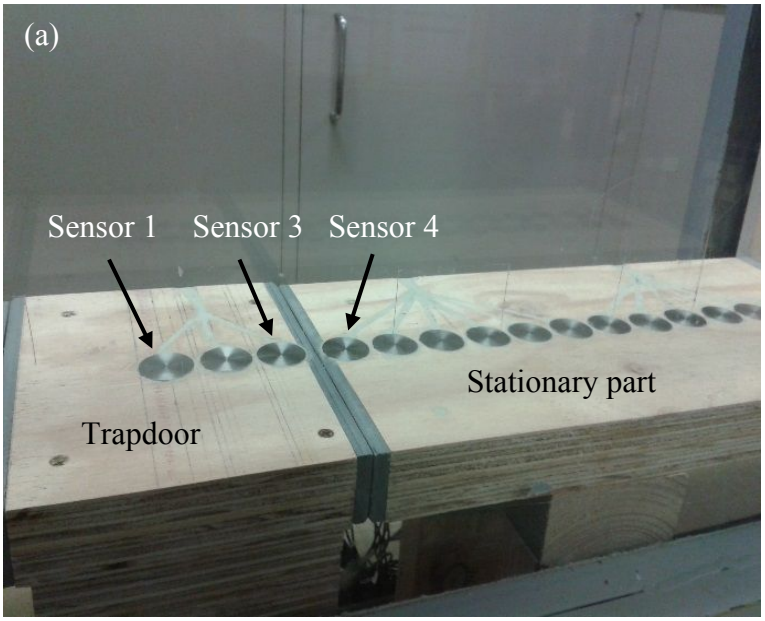

153

154

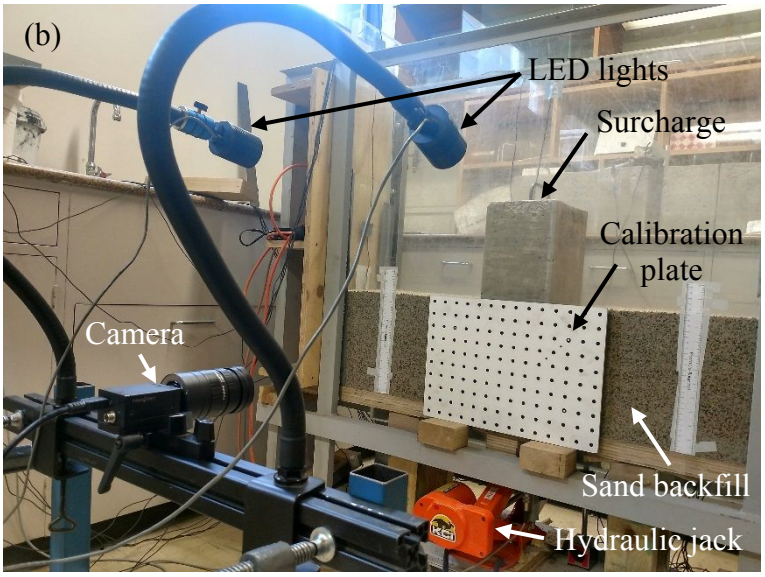

155

156 Fig. 1. The instrumented trapdoor apparatus: (a) stress sensor array, (b) imaging equipment

157

158 The trapdoor apparatus was instrumented with a series of pressure sensors. The
159 sensors, 28 mm in diameter, were secured into rebates fabricated into the base board, and
160 flush with the board surface. This arrangement minimised material deformation errors
161 associated with the measurement process. As the trapdoor apparatus represents axisymmetric,

plane-strain conditions, the pressure sensors were placed on only one side of the apparatus. The trapdoor element had three sensors installed at centre (Sensor 1), intermediate (Sensor 2) and edge (Sensor 3) locations. The centre-to-centre distance of the sensors, or sensing interval, was 30 mm. The numbering of the sensors continued from the edge of the stationary part, from Sensor 4 to Sensor 15 which was placed 420 mm away from the edge. The sensors were calibrated using a Fluke-100g electric pressure calibrator. A data acquisition system and an associated computer program were used to record the sensor readings with a sampling rate of 16 Hz. This sampling rate was equal to that of the trapdoor LVDT and, given the displacement rate of the hydraulic jack, ensured that the pressure sensors recorded the stress data at intervals of 0.2 mm of the trapdoor displacement. The LVDT and the pressure sensor recordings were synchronised within the data acquisition system. More details on the stress measurement using the pressure sensors are provided by Khatami et al. (2019).

After preparing the backfills in the trapdoor apparatus, according to the procedure outlined earlier, recording sessions were conducted to capture images of each backfill surface as the deformation progressed. The system, which included the photographic equipment shown in Fig. 1(b), VicSnap software for imaging, and the VIC-2D program for image correlation analysis were supplied by Correlated Solutions, USA. A machine vision camera with conventional charge-coupled device (CCD) technology, equipped with a low distortion 75 mm Fujinon lens and aperture size range of 1/22–1/2.8, was used for imaging. An area of interest (AOI) was defined where most of the significant deformations were expected to take place. The AOI measured 500 (W) × 250 (D) mm. The image recording sessions were completed with a capture rate of 160 frames per second and a resolution of 960 × 600 pixels, using the VicSnap program. To convert the pixel scale information in the images to the more suitable physical unit of mm, scale calibration was carried out using the dot grid calibration target shown in Fig. 1(b). After calibration, a pixel to millimetre ratio of 0.52 was obtained.

The images were then analysed to measure deformation using the VIC-2D program, which computes displacements and strains from an image correlation algorithm. The image correlation procedure in the DIC technique involves taking a reference image of each specimen in an undeformed state at the beginning of the tests. The AOI regions in the reference images are then discretised into a grid of squared blocks, known as subsets. The speckle pattern applied in the sample preparation phase helps to identify and distinguish each subset, provided that the speckle pattern in each subset is unique. The new location of each subset in the subsequently captured images of the deforming specimen is tracked in terms of the greyscale intensity values of each of the subset pixels. The displacement of the subsets, and thus the displacements and strains that take place in the AOI, are then calculated, while the image correlation criterion is satisfied. The detailed mathematics of the DIC technique is well documented in the literature (e.g. Pan et al., 2008; Schreier et al., 2009) and is not discussed further here in the interests of brevity. In the present study, a subset size of 21 × 21 pixels (equivalent to an area of approximately 11 mm × 11 mm) was used. This size rendered the AOI into a grid of distinguishable subsets while minimising noise in the output data or an unnecessary increase in computational time. The computer unit used in this study was equipped with a dedicated graphics card of 16 GB memory. As a result, the image processing speed was about 25 minutes per 1,000 images.

3. Results and discussion

The passive arching tests were conducted with and without the applied surcharge. In addition to the rubber–sand mixtures, sand specimens were tested as a control. The test results included the distributions of displacements, strains and stresses obtained across the AOI of each specimen for a trapdoor displacement of 2 mm.

3.1. Horizontal displacements and horizontal strains

The horizontal displacements (u) of the Sand and rubberised sand backfills induced by the upward movement of the trapdoor, with no surcharge and with the 5 kPa central surcharge, are shown in Figs. 2 and 3 respectively. The horizontal displacements to the right-hand side of the symmetric axis of the apparatus are positive as illustrated in Fig. 2(a). When no surcharge was applied (Fig. 2), the vertical translation of the trapdoor caused the particles at the surface and at shallow depths to displace horizontally from their original position towards the sides of the stationary parts. The peak values of the horizontal displacements created two semicircles immediately below the surface, as shown in Fig. 2. The averaged peak values from the left and right sides of the graphs were reduced from 0.65 mm in the Sand to 0.58 mm, and 0.42 mm in the 10% and 30% Rubber backfills, respectively. This difference will naturally increase as the model is up-scaled in line with actual backfilled systems. This means that the rubber inclusions help reduce horizontal swell where passive arching occurs. The rubber inclusions, however, also broadened the zones of swell. The distribution of horizontal swell changed in location, shape and depth, when the surcharge was applied, as shown in Fig. 3. The zones of peak swell relocated outward slightly, avoiding contact with the surcharge, but increased in size when compared with the corresponding results obtained without the surcharge. The zones of peak swell extended with the increase of rubber content. Compared with the results in Fig. 2, the maximum horizontal displacements increased to 0.90 mm in the Sand backfill, while remaining unchanged in the rubberised backfills. Similar to the no surcharge case, the zones of peak swell extended when the rubber content increased.

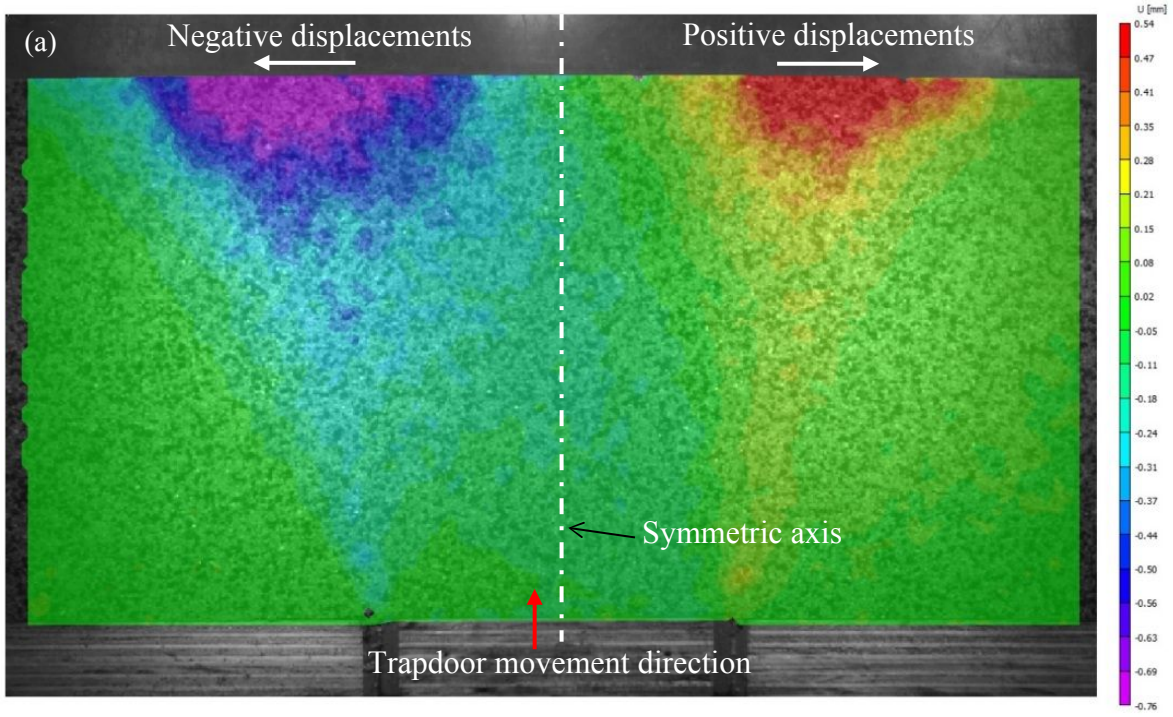
(a)
Negative displacements
Positive displacements
Symmetric axis
Trapdoor movement direction
U [mm]
0.54
0.47
0.41
0.35
0.28
0.21
0.15
0.08
0.02
-0.05
-0.11
-0.18
-0.24
-0.31
-0.37
-0.44
-0.50
-0.56
-0.63
-0.69
-0.76

235

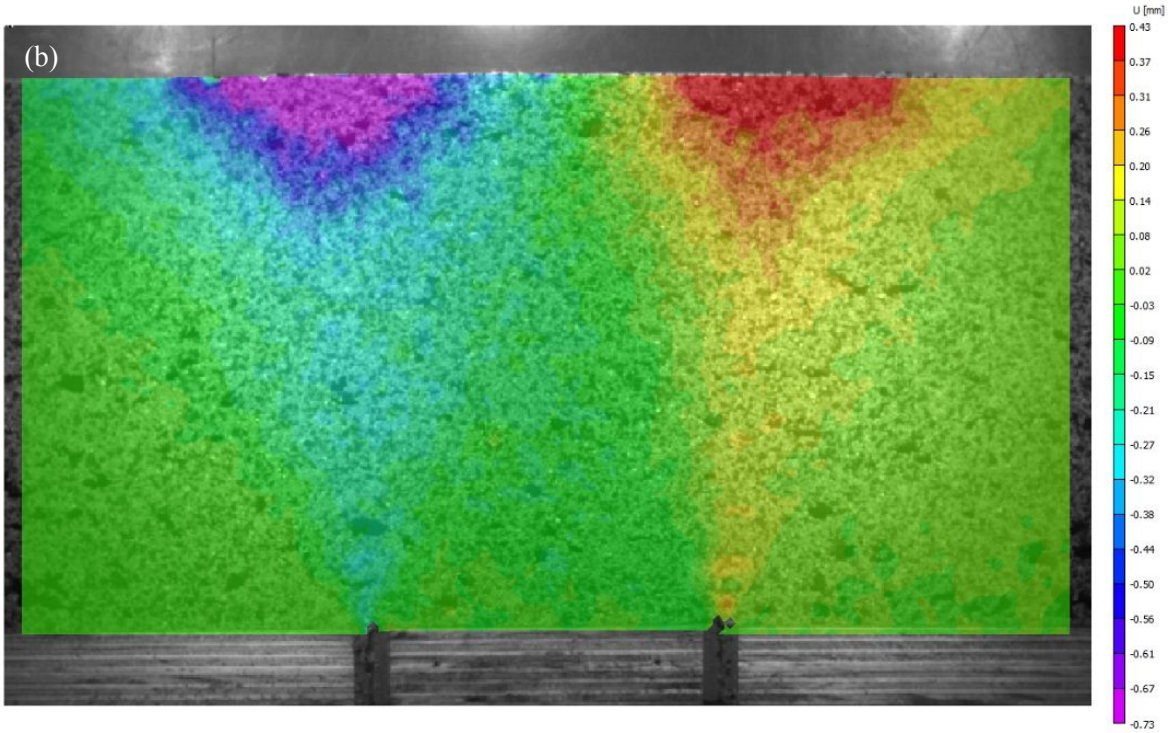
(b)
U [mm]
0.43
0.37
0.31
0.26
0.20
0.14
0.08
0.02
-0.03
-0.09
-0.15
-0.21
-0.27
-0.32
-0.38
-0.44
-0.50
-0.56
-0.61
-0.67
-0.73

236

237

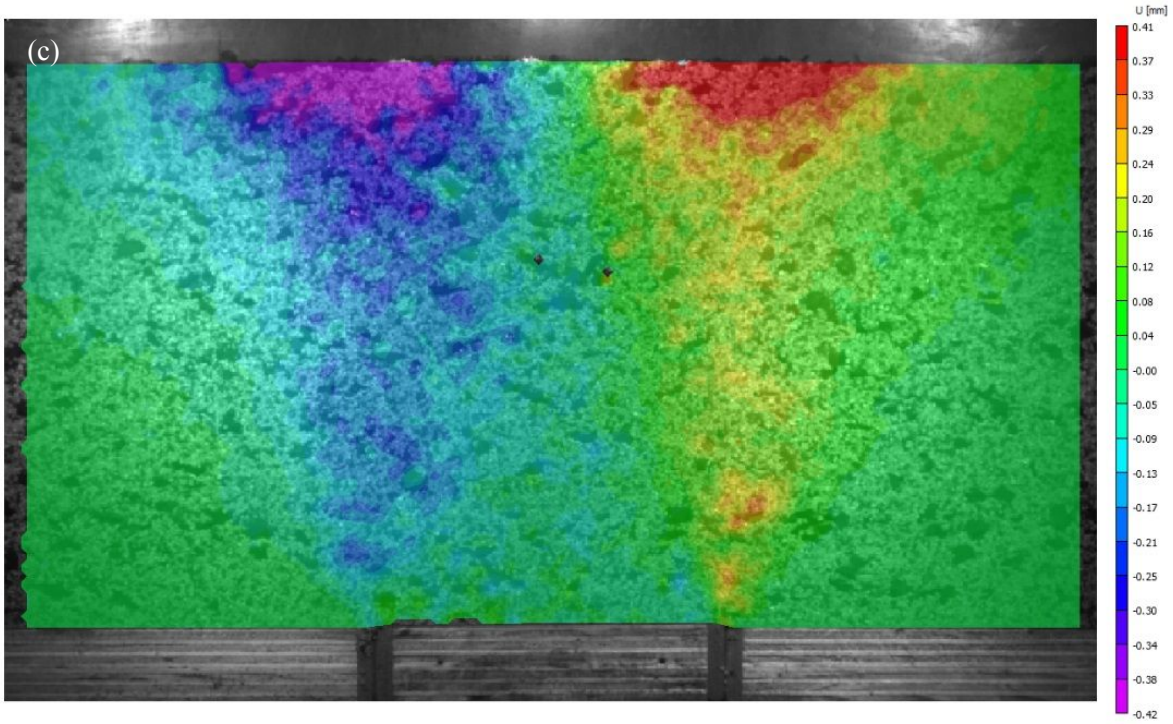

238

239 Fig. 2. Distribution of horizontal displacements under no-surcharge conditions for the three

240 materials: (a) Sand, (b) 10% Rubber–sand, and (c) 30% Rubber–sand

241

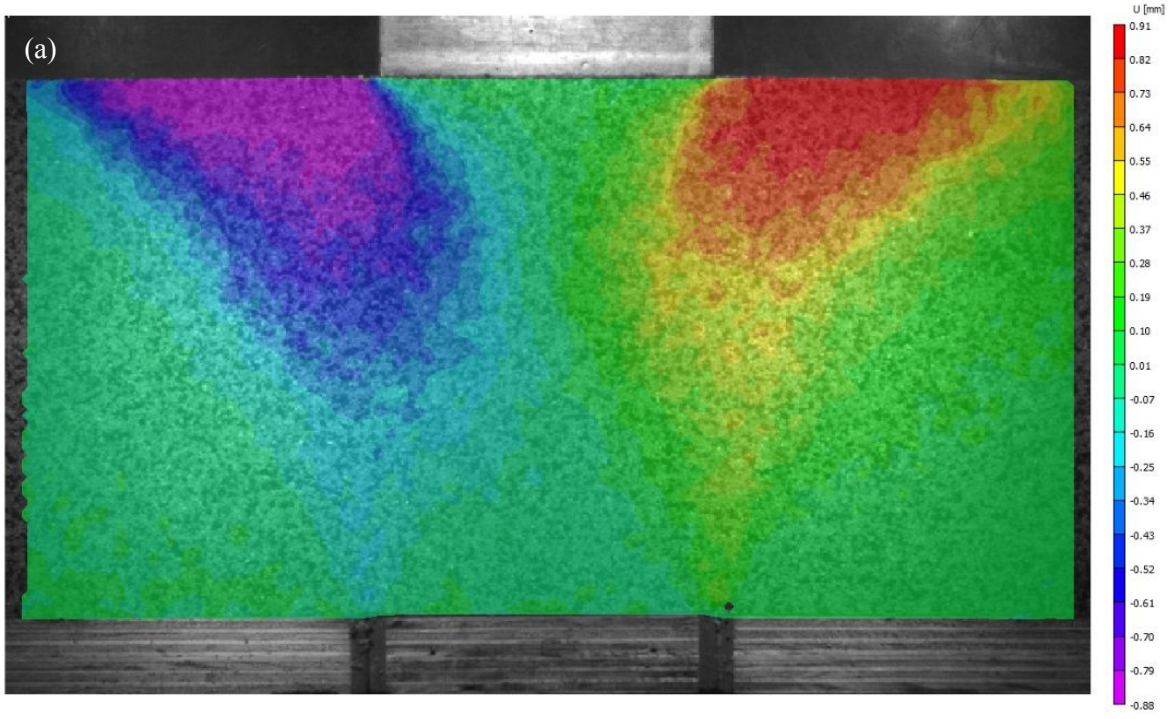

242

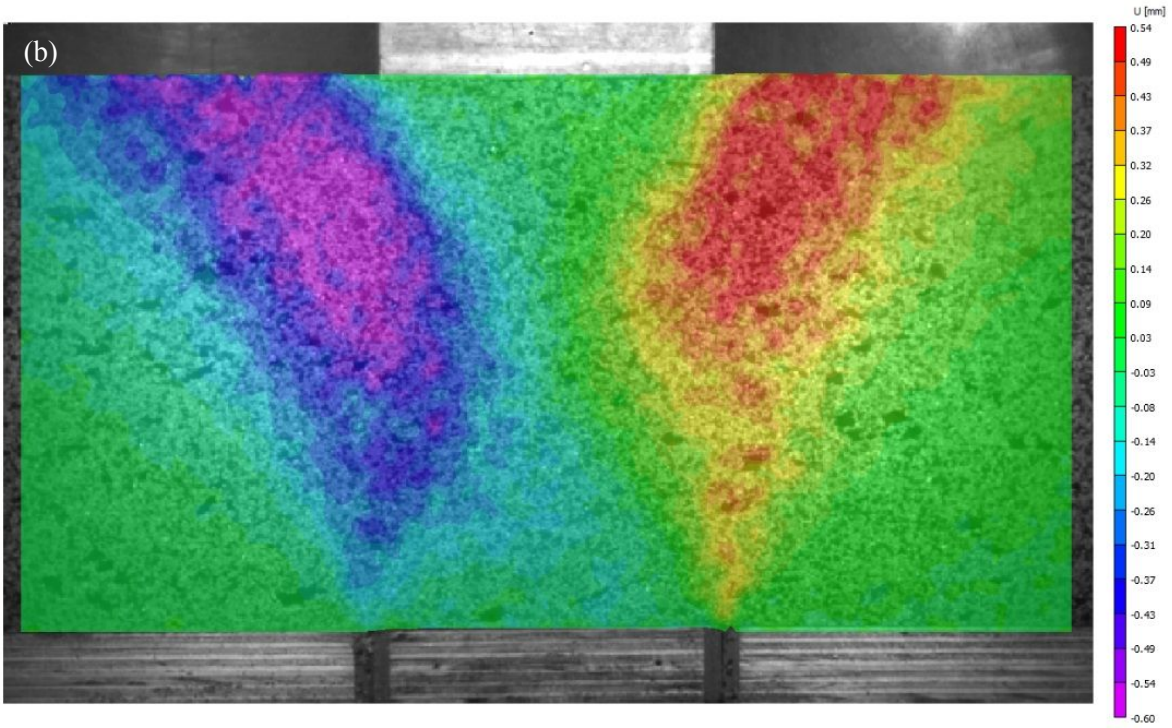

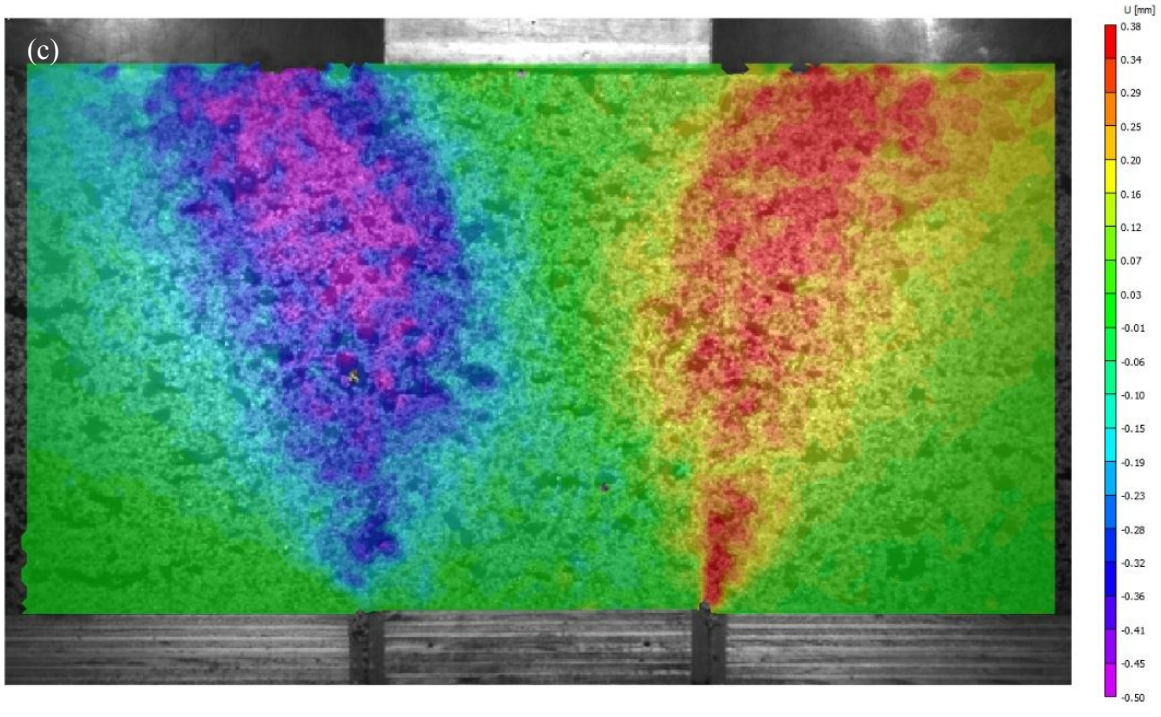

Fig. 3. Distribution of horizontal displacements with the application of the 5 kPa surcharge for the three materials: (a) Sand, (b) 10% Rubber–sand, and (c) 30% Rubber–sand

The distributions of horizontal strains (ε_{xx}) in the backfills subjected to no surcharge and with the application of the 5 kPa surcharge are presented in Figs. 4 and 5 respectively. As can be observed, under all testing conditions, tensile strains governed the central areas. The tensile areas were sandwiched by areas of compressive strains, which include the peripheral wedge areas enveloping the tensile regions. The wedge areas initiated from the edges of the stationary parts and expanded progressively and outwardly towards the surface. Immediately above the trapdoor is a zone of null horizontal strains, forming a trapezoidal shape. The height of the trapezoid decreased as the rubber content increased, or the surcharge was applied. In each backfill, the extent of the horizontal strains was greater under the surcharge condition than with no application of surcharge, where the materials remained the same. Figs. 4 and 5 also indicate that the AOIs increased with rubber content and the application of the surcharge. The AOI became greatest in the case of the 30% Rubber–sand under surcharge loading [Fig. 5(c)], where almost the entire AOI exhibits strain.

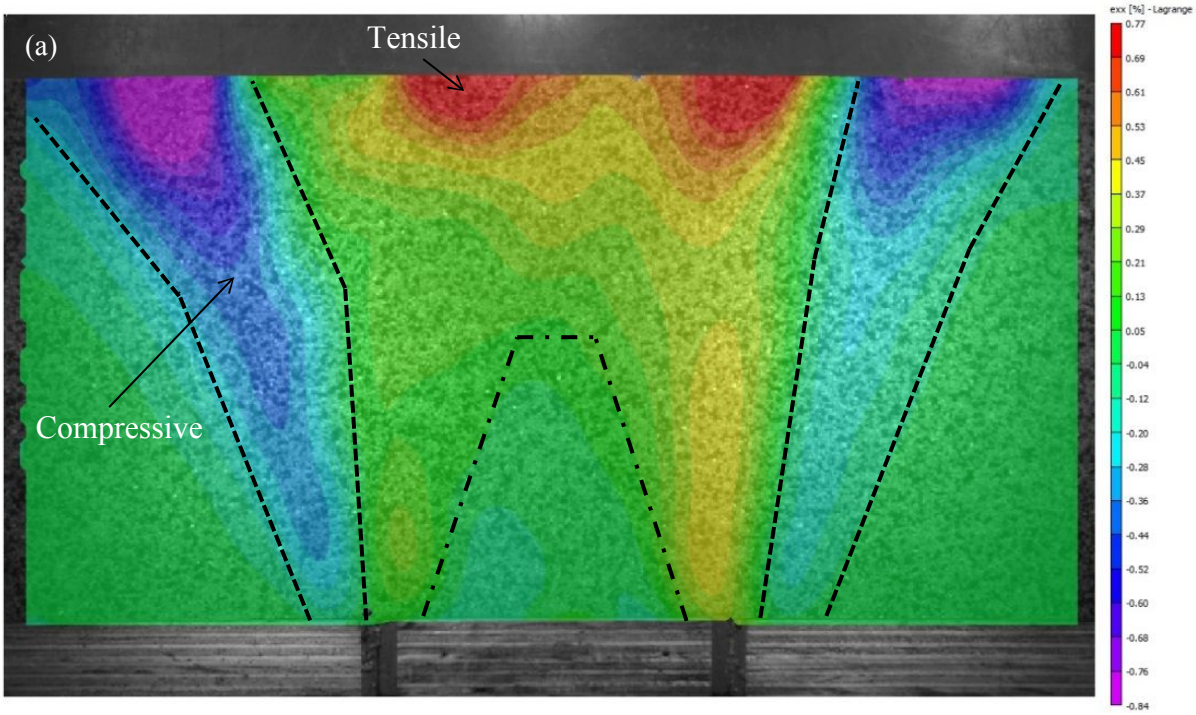

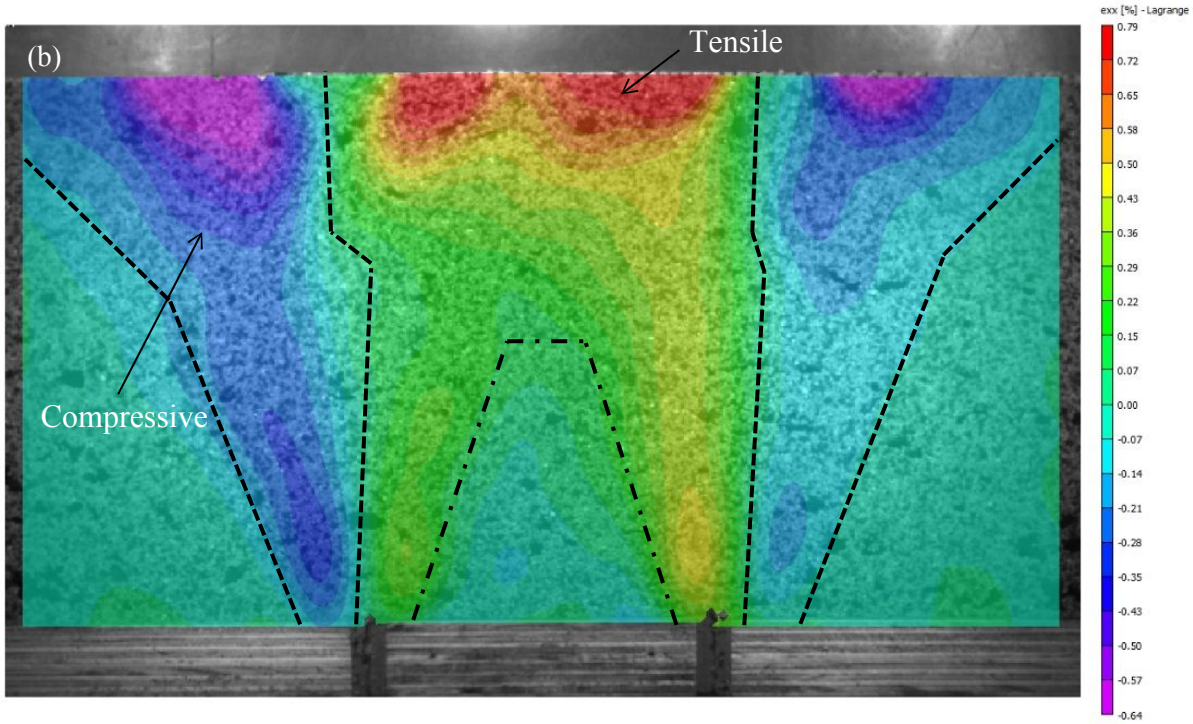

264

265

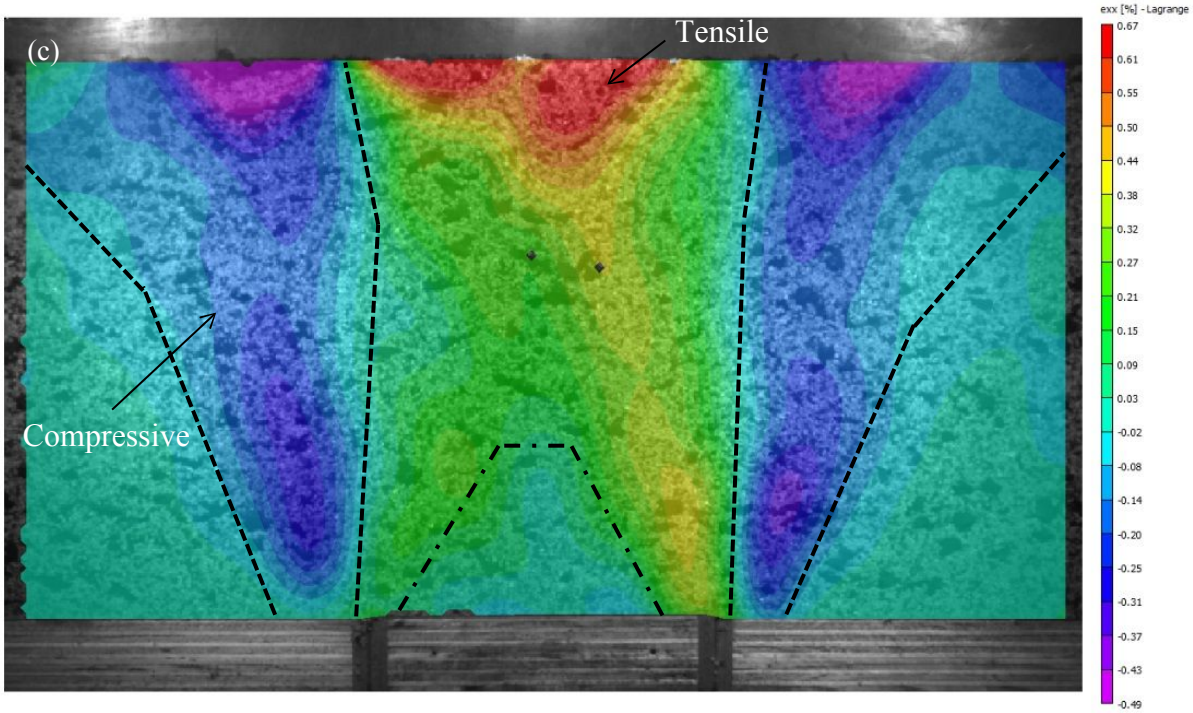

266

267 Fig. 4. Horizontal strain distributions under no surcharge conditions for the three materials:

268 (a) Sand, (b) 10% Rubber–sand, and (c) 30% Rubber–sand

269

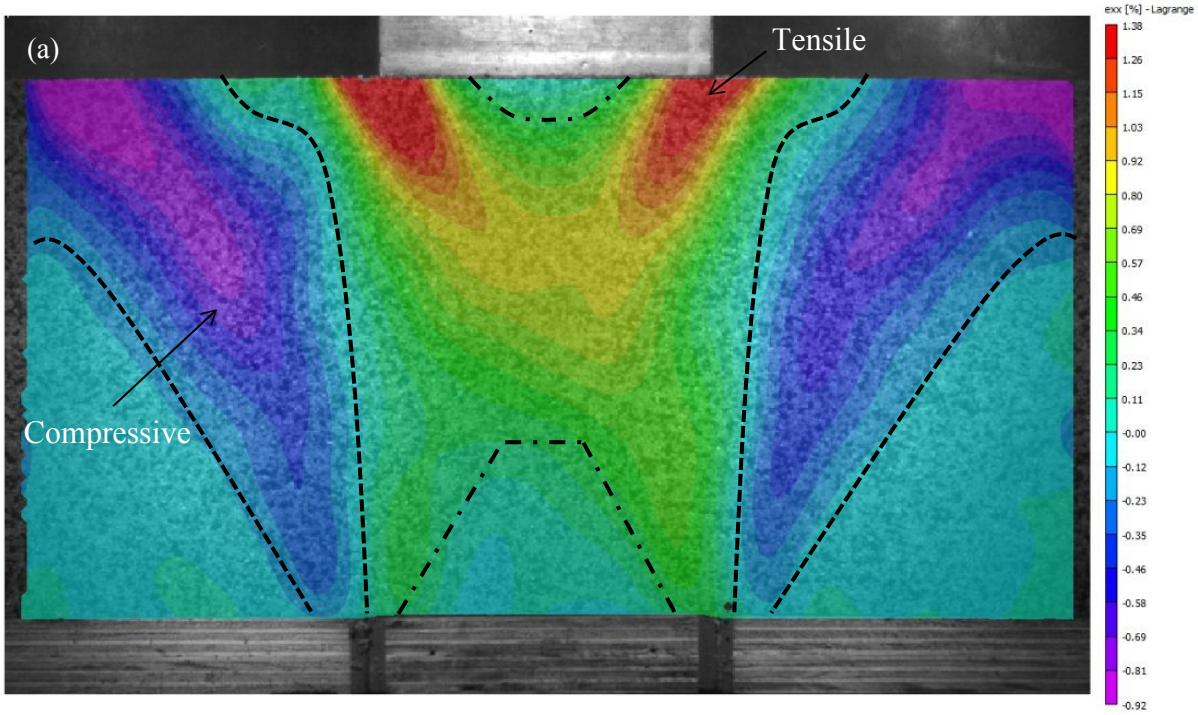

270

271

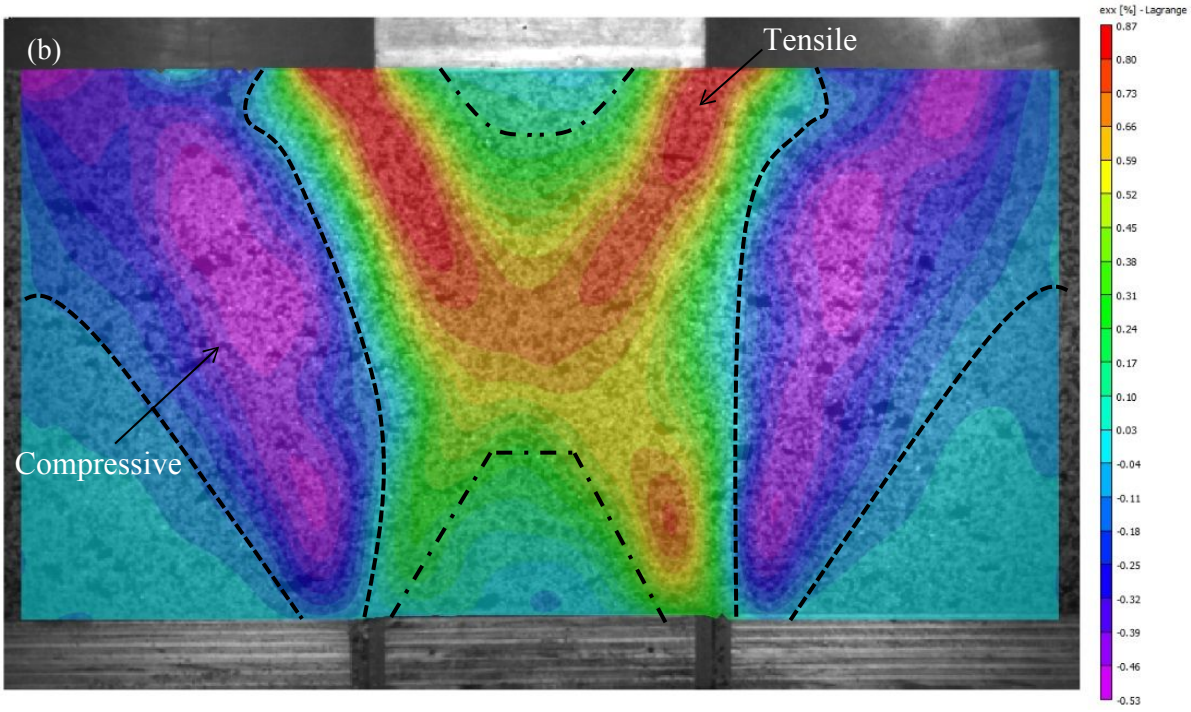

272

273

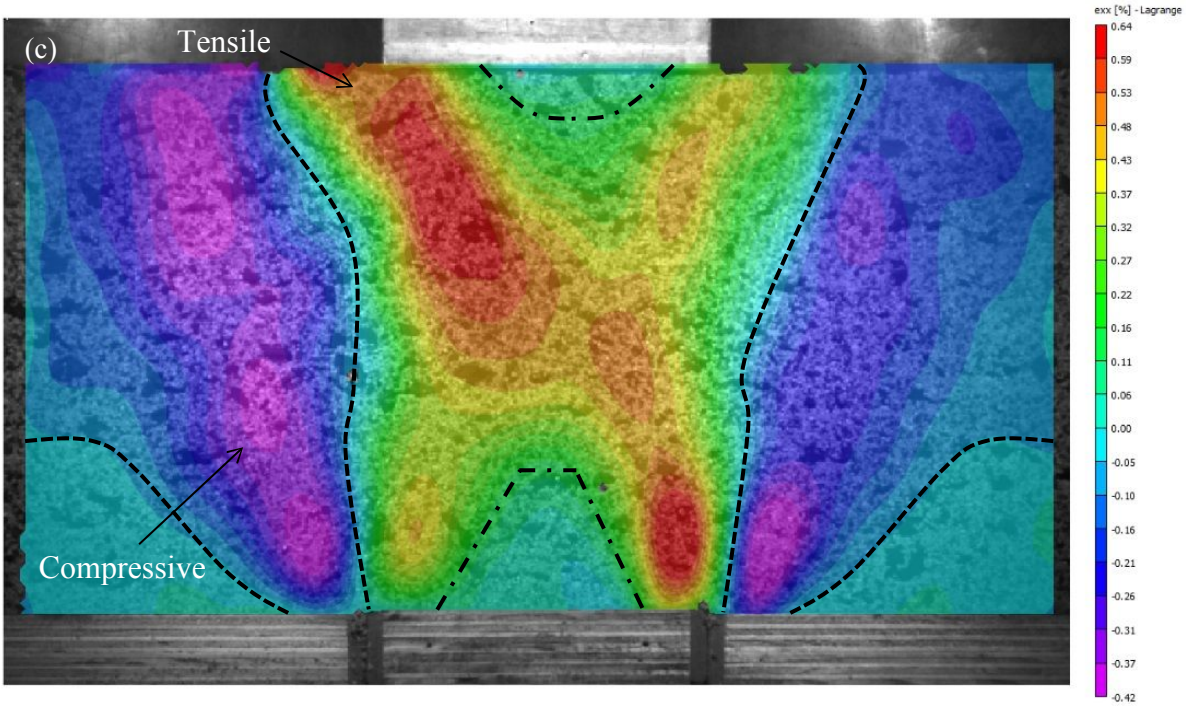

Fig. 5. Horizontal strain distributions with the application of surcharge for the three materials: (a) Sand, (b) 10% Rubber–sand, and (c) 30% Rubber–sand

The maximum tensile and compressive horizontal strains decreased with increased rubber content, whereas the other characteristics remained unchanged. For example, under the no surcharge condition, the maximum compressive horizontal strains reduced from a maximum of 0.84% in the Sand backfill to 0.64% for the 10% Rubber–sand backfill and 0.49% for the 30% Rubber–sand backfill. For the Sand backfill, the use of the surcharge increased from 0.84% to 0.92%, for the peak compressive horizontal strain, and from 0.77% to 1.38% for the peak horizontal tensile strain. However, the opposite occurred to the rubberised backfills. The use of the surcharge reduced the horizontal strains on average by 0.13% for the 10% Rubber–sand backfill and by 0.05% for 30% Rubber–sand backfill. As Figs. 4 and 5 show, when the surcharge block was applied, the peak compression values were reduced. The reason for this observation is that the local surcharge directed the deformations

toward the vertical orientation while increasing the intensity of the tensile horizontal strains. The measurements presented in Figs. 2–5 show that the backfill deformation extends laterally to greater areas with the rubber inclusions and the use of surcharge. However, the peak tensile and compressive horizontal displacements and strains were reduced by the rubber inclusions. As the stiffness of rubber is significantly lower than that of sand, the addition of rubber to sand decreased the overall stiffness of the rubber–sand mixtures. This means that more deformation is needed for rubberised sand to mobilise its peak strength. On the other hand, the Poisson's ratio of rubber is approximately 0.5, which is the maximum value of Poisson's ratio of a material, and mixing rubber with sand resulted in an increased Poisson's ratio of the geomaterials. The combined effect of these two phenomena have possibly led to reduced peak strains and increased extension of the deformed area.

3.2. Vertical displacements and vertical strains

The distribution of vertical displacements (v) mapped for Sand and Rubberised–sand under no surcharge and the application of surcharge are presented in Figs. 6 and 7 respectively. When the trapdoor rose, the layers were divided into three zones depending on the level of displacement. The first zone (Zone 1), identified in red in Figs. 6 and 7, comprised an assembly of particles that shifted upwards together with the trapdoor. As the displacement remains the same as that of the trapdoor, this zone is termed the 'arch of equal displacement.' The second zone (Zone 2), highlighted in purple, comprised of two rigid bodies, above the stationary parts of the apparatus, where the vertical displacements were negligible. Finally, the third zone (Zone 3), intermediate between the two sets of rigid bodies having negligible and the greatest displacements, was created by the relative displacements of these rigid bodies with respect to each other. This is a zone of transition, implying that the displacements ranged from effectively zero to a value close to the displacement of the

trapdoor. Application of the central surcharge notably affected the distribution of vertical displacements. In the rubberised backfills, in particular, an inverted arch-shaped region appeared beneath the surcharge block. The values of vertical displacements in this region were in the range of 0.6–0.7 mm, in the low rubber content backfill, and reduced to 0.2–0.3 mm in the high rubber content backfill. The idealised boundaries of Zones 1, 2, and 3 are presented in Figs. 6–7.

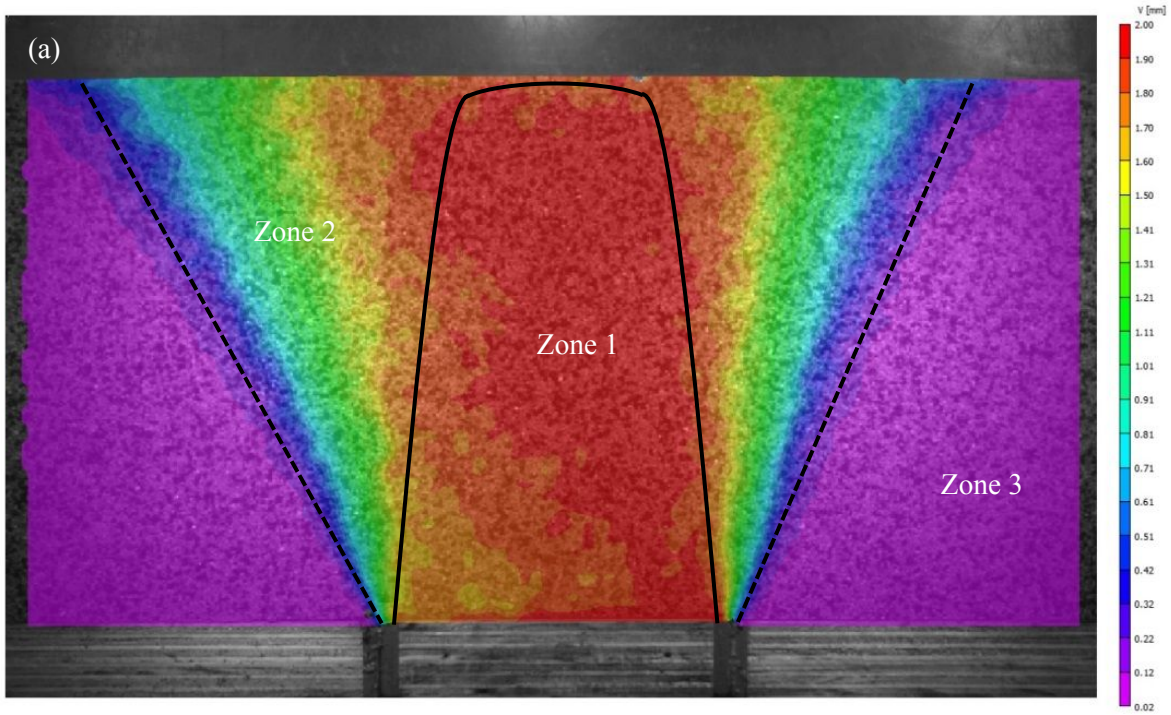

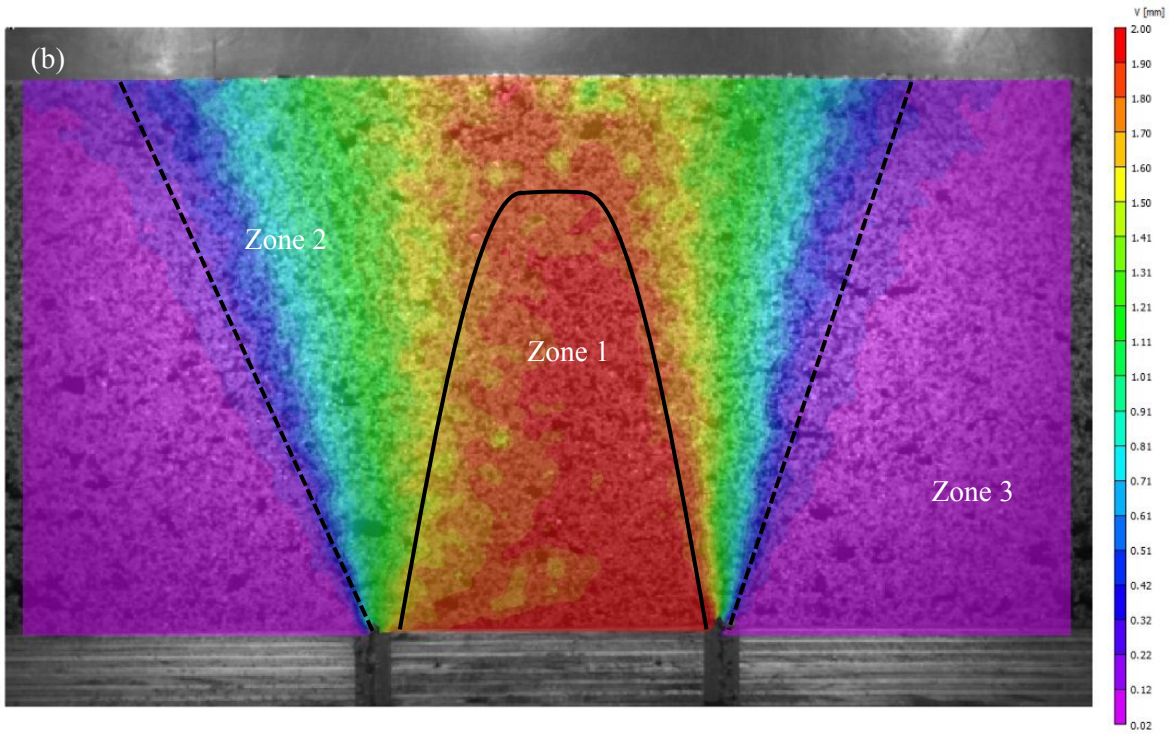

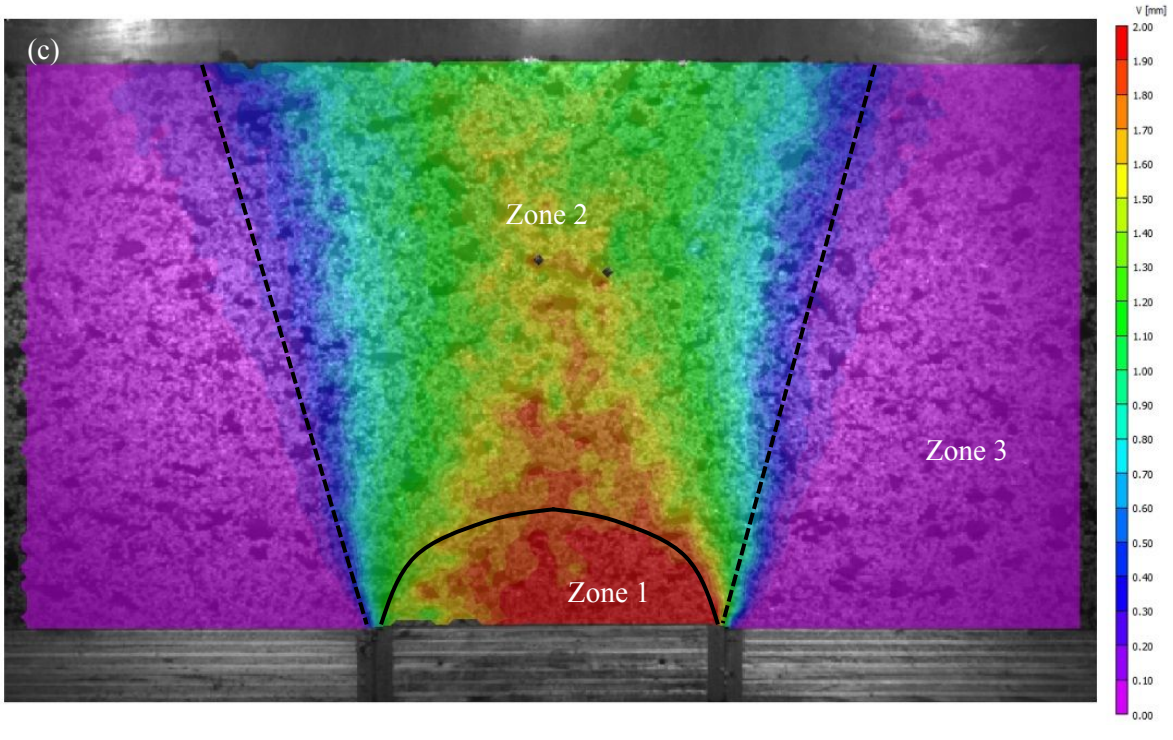

Fig. 6. Distributions of vertical displacements under no surcharge conditions for the three materials: (a) Sand, (b) 10% Rubber–sand, and (c) 30% Rubber–sand

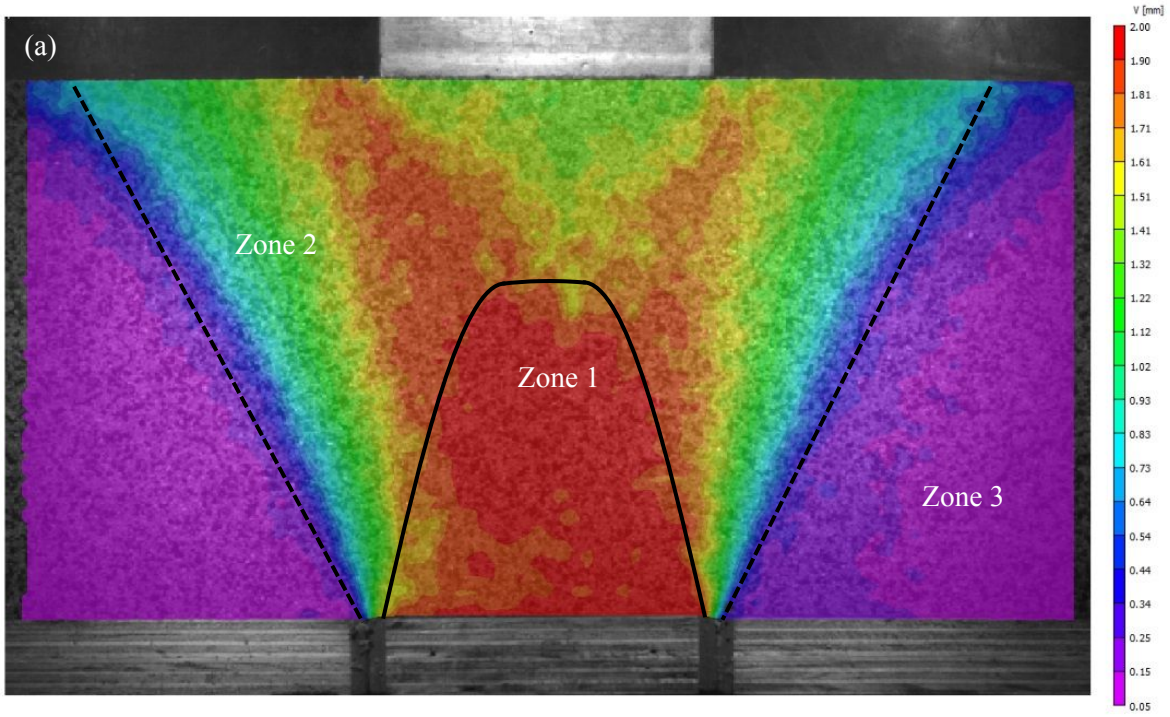

329

330

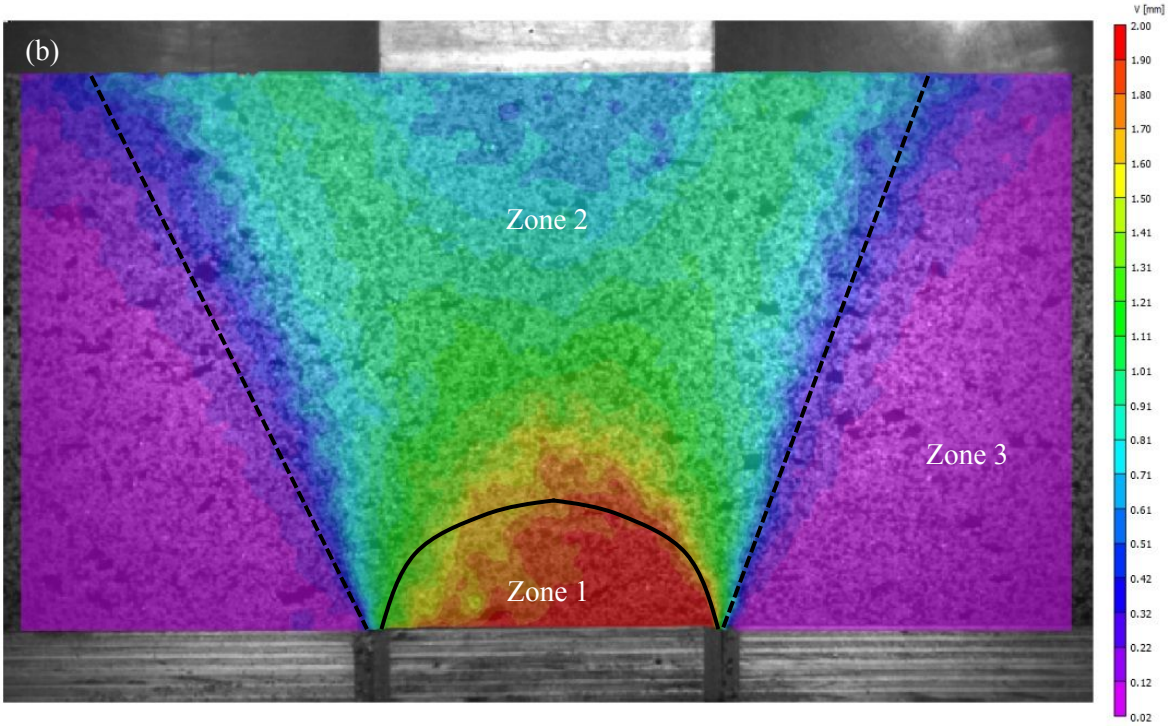

331

332

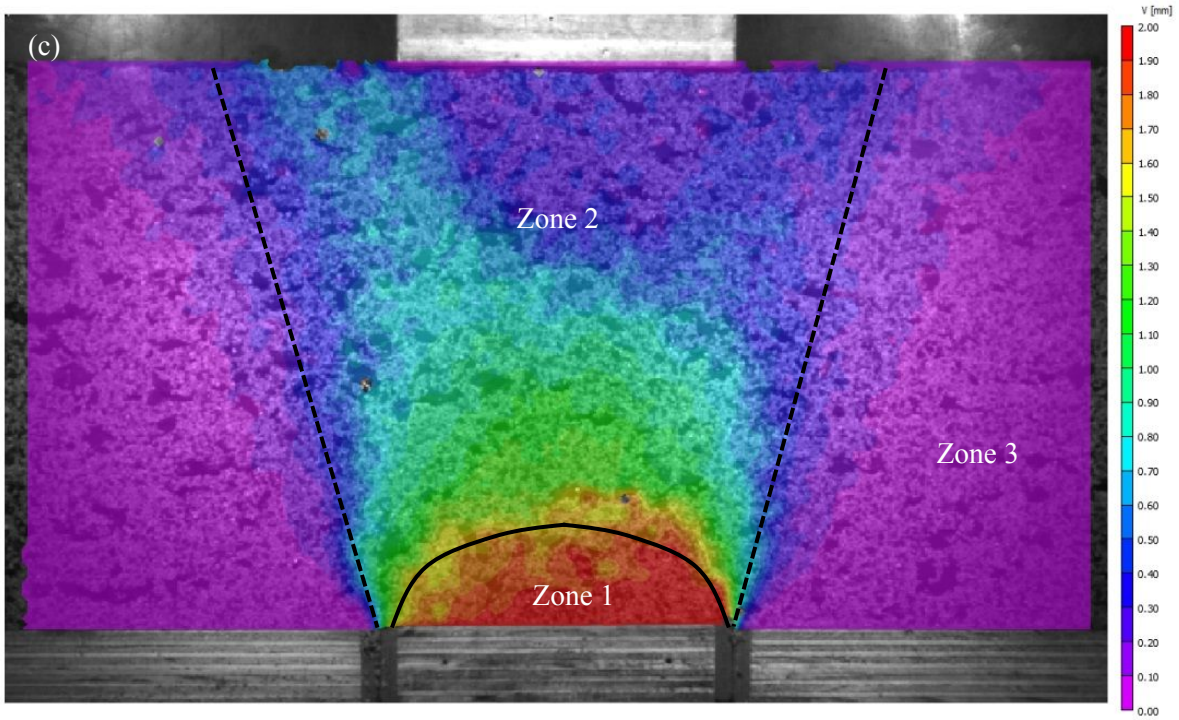

333

334 Fig. 7. Distributions of vertical displacements with the application of surcharge for the three
335 materials: (a) Sand, (b) 10% Rubber–sand, and (c) 30% Rubber–sand

336

337 Zones 1 and 3 can be combined and idealised into an inverted isosceles trapezoid
338 forming the total arch area. To examine the effects of rubber inclusions on the evolution of
339 the arches, the area of the arches was measured, and the results are provided in Table 2 in the
340 form of the area of the arch, and the normalised height of the arches of equal displacement
341 with respect to the trapdoor width. The arch height was measured vertically from the centre
342 of the trapdoor on the geomaterial-trapdoor interface to the tip of the arch in Zone 1. It is
343 evident that the area of the trapezoids decreased with increased rubber inclusion, and the
344 coverage decreased roughly by 5%, depending on the rubber content and in the situation
345 where the surcharge condition remained the same. With the application of the surcharge, the
346 area of the arch increased by 5.5% for Sand, 5.7% for 10% Rubber–sand, and 6.3% for 30%

Rubber–sand. On the other hand, the application of the surcharge reduced the side slopes of the arch, thus deforming the arches outward.

Table 2. Area of arch and crest height of the arch of equal displacement in different backfills

Test conditions	Material	Total arch area (mm^2)	Percentage of AOI covered	Normalised arch height (%)
No surcharge	Sand	74,625	59.7	153
	10% Rubber	69,375	55.5	125
	30% Rubber	62,688	50.2	32
With surcharge	Sand	78,722	63.0	92
	10% Rubber	73,325	58.7	39
	30% Rubber	66,663	53.3	24

Rubber inclusions also lowered the crest of the arches of equal displacement. As shown in Table 2, the crest diminished by 28% of the trapdoor width for 10% Rubber–sand, and 121% for 30% Rubber–sand, for the no surcharge case. A similar trend was observed in the case of surcharge loading. The effect of surcharge on the variation of the crest was more pronounced in the Sand and 10% Rubber–sand than in the 30% Rubber–sand. Specifically, the surcharge reduced the arch crest by 61% of the trapdoor width in the Sand and 86% in 10% Rubber–sand, but only by 8% in the 30% Rubber–sand. Figs. 6 and 7 and Table 2 suggest that adding rubber to the sand helped reduce the area of arching. A similar reduction occurred when the surcharge was applied.

The distributions of vertical strains (ε_{yy}) in the Sand and Rubberised–sand, when subjected to passive arching with no surcharge and under surcharge loading, are presented in Figs. 8 and 9 respectively. In each of the backfills, the tensile strains originated from the

trapdoor edges and formed two outwardly oriented bands which extended up to the surface. The tensile bands gradually increased as they evolved up to the surface and became noticeably thicker at the surface when the surcharge was applied. The greatest vertical tensile strains occurred in the Sand. The strains were 1.2% with no surcharge and 0.6% under the application of the surcharge. This suggests that rubber inclusions reduce the peak vertical strain arising from arching. Specifically, adding 10% rubber reduced the strain by approximately 50%, whether the surcharge was applied or not. Adding 30% rubber further reduced the strains by approximately 15% in the no surcharge case, and by 20% with surcharge compared to the 10% rubber content backfill.

Vertical compressive strains were also mapped along the cross-sections of the backfills, as shown in Figs. 8 and 9. In all cases, the compressive regions were bounded by the bands of tensile strain. The maximum compressive strains fell into a narrow range of 0.7–0.8% for all no-surcharge cases. When the surcharge was applied, the peak values of compressive strains increased by up to 0.4%, but nevertheless fell into a narrow range of 1–1.1%. It is noteworthy that a band of compressive strain formed beneath the surcharge block [Fig. 9(c)]. Closer examination of this band highlighted the presence of concentrated rubber particles which resulted in a small degree of heterogeneity. Furthermore, the backfill layers near the surface are usually, moderately less compacted when compared to the deeper layers, due to the reduced overburden weight. Therefore, this band beneath the surcharge block experienced significantly higher compressive vertical strains in comparison to the rest of the backfill. The distributions in Figs. 8(c) and 9(c) emphasise the importance of homogeneity and appropriate compaction of rubberised backfills.

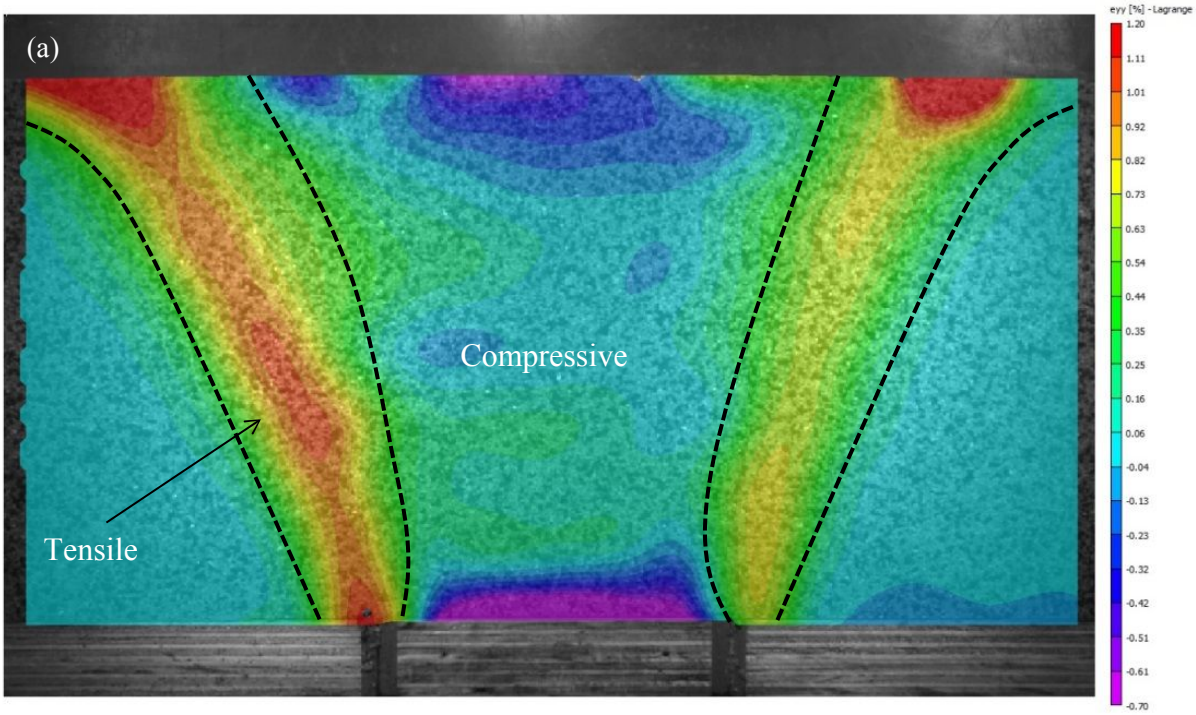

387

388

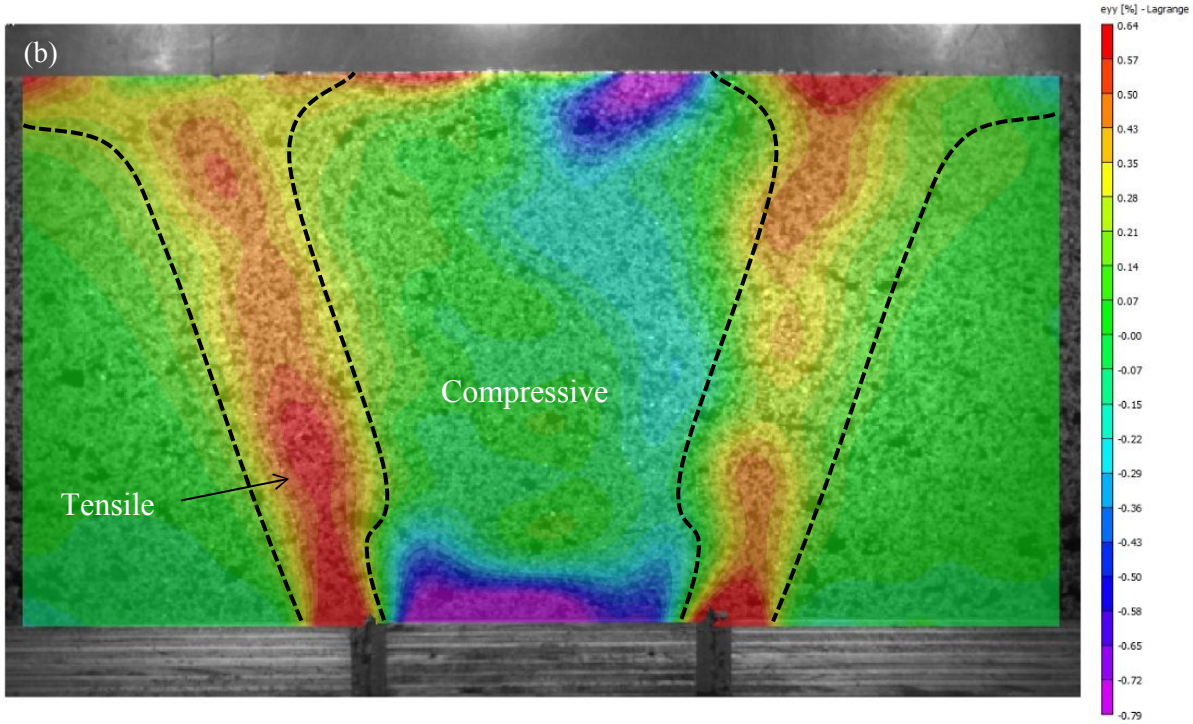

389

390

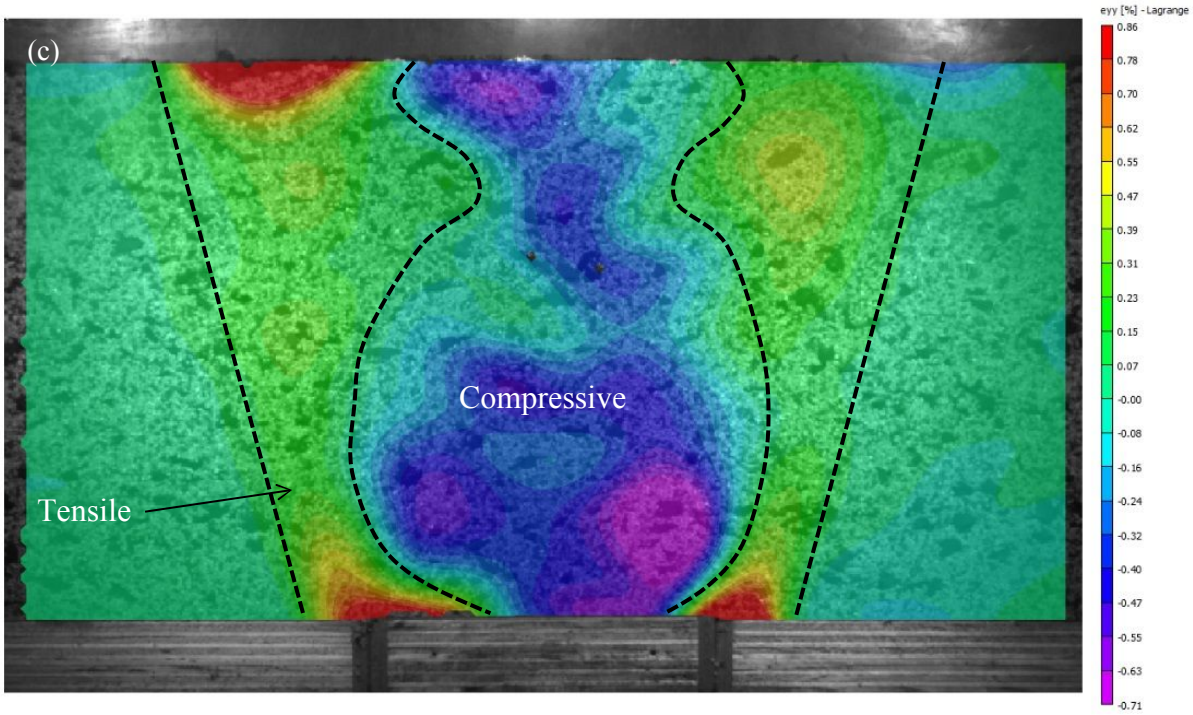

Fig. 8. Vertical strain distributions under no surcharge for the three materials: (a) Sand, (b) 10% Rubber–sand, and (c) 30% Rubber–sand

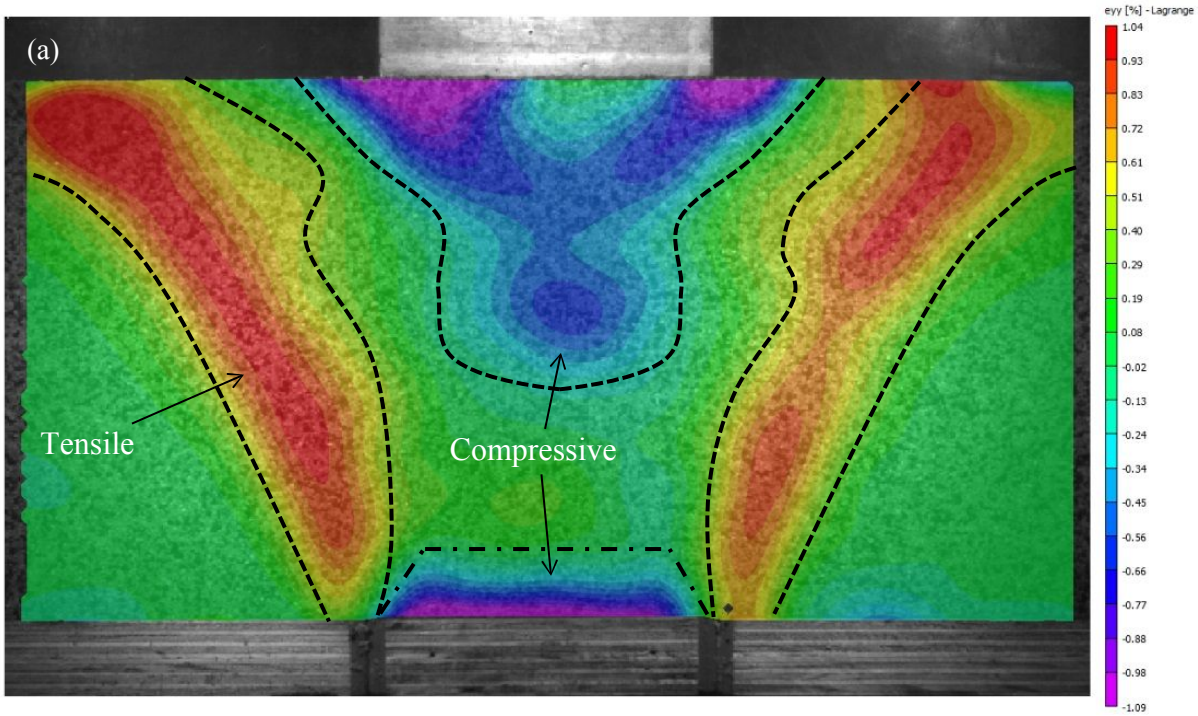

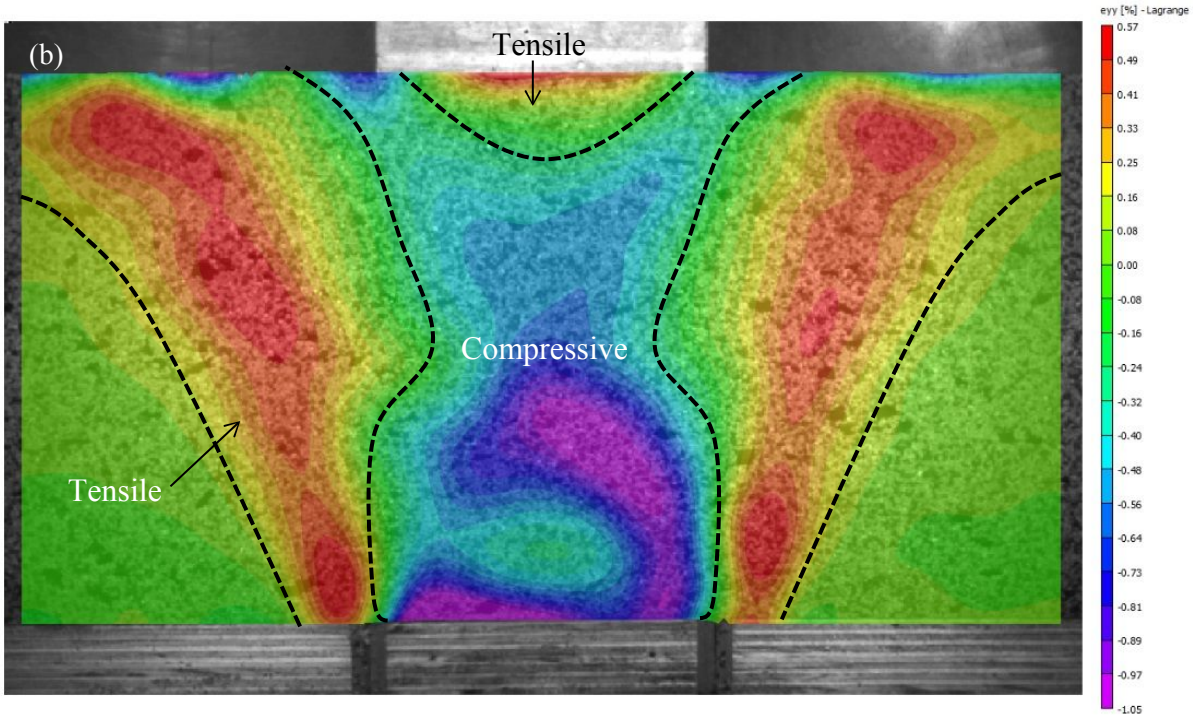

397

398

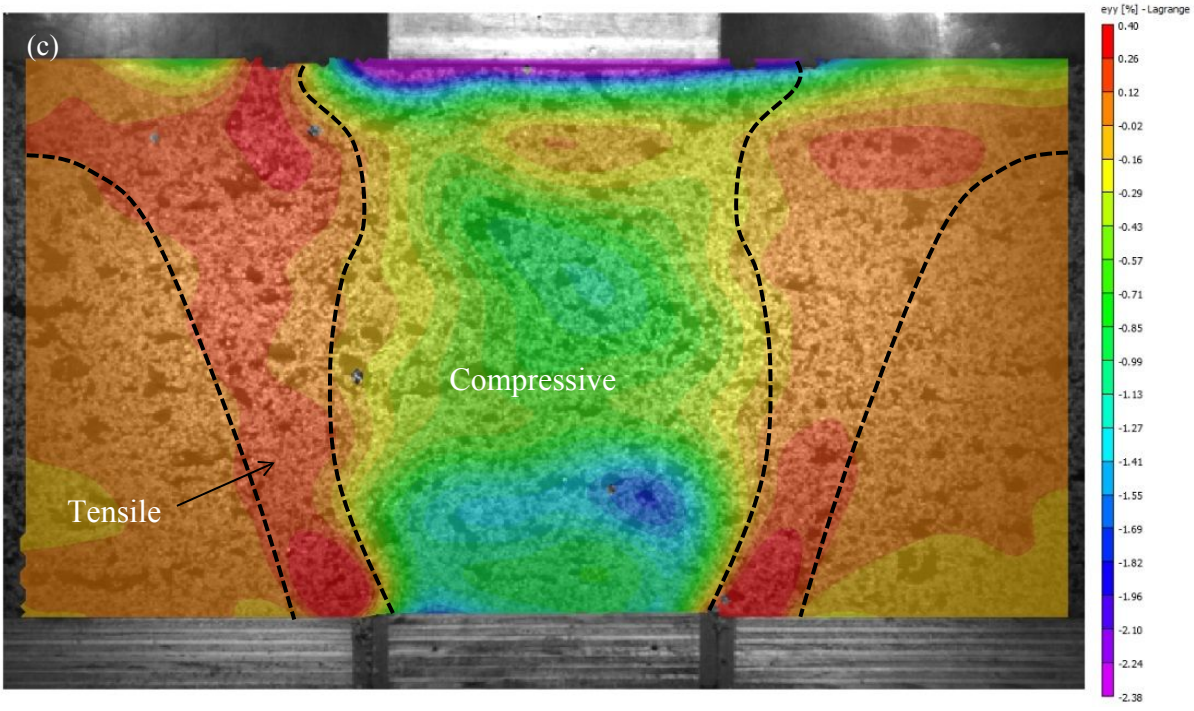

399

400 Fig. 9. Vertical strain distributions with the application of surcharge for the three materials:

401 (a) Sand, (b) 10% Rubber–sand, and (c) 30% Rubber–sand

402

3.3. Shear strains and shear bands

The distribution of shear strains (ε_{xy}) developed in the Sand and rubberised backfills under passive arching with no surcharge and with the application of the 5 kPa surcharge are presented in Figs. 10 and 11 respectively. The intensity of shear straining was generally reduced when rubber was mixed with sand. In the no surcharge cases, the average value of the maximum shear strains decreased from 1.65% in the Sand to 1.53% in the low rubber-content backfill, and to 1.37% in the high rubber-content backfill. The application of surcharge decreased the corresponding maximum values. In this case, with the addition of rubber to the Sand, the average maximum shear strains reduced to from 1.4% to 1.2% in both rubberised backfills. Shear strains therefore decreased when the Sand backfill was rubberised. Both 10% and 30% rubber content backfills showed similar shear deformability under surcharge loading.

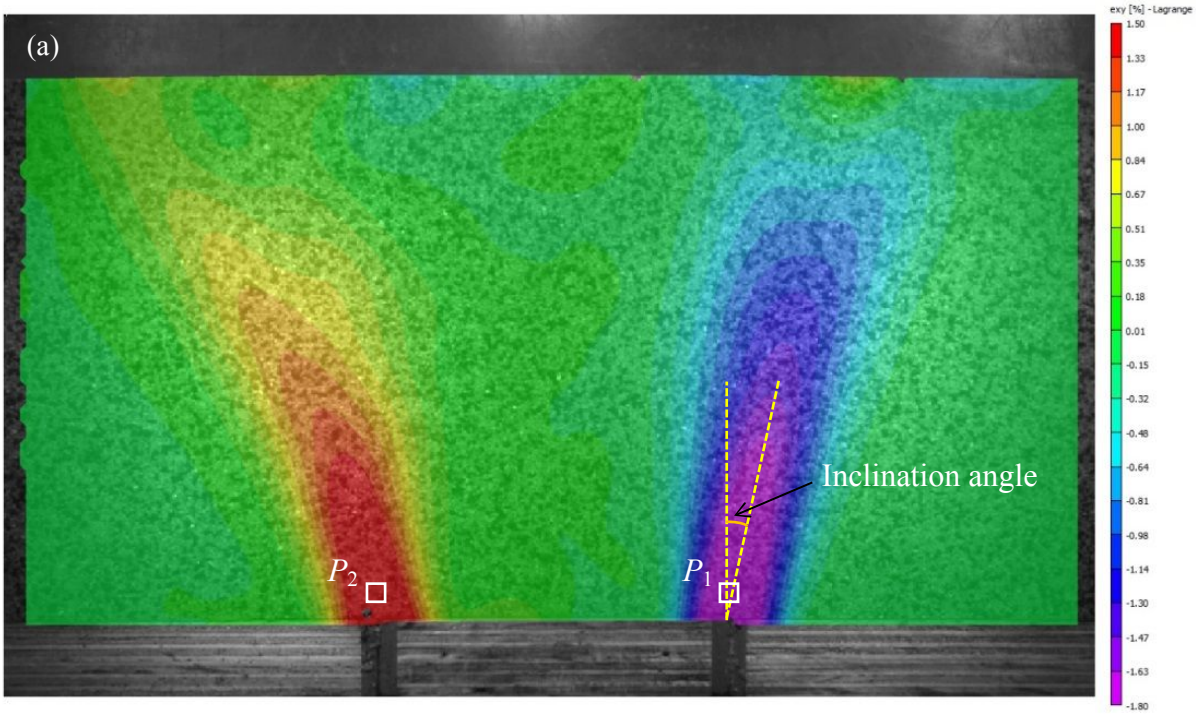

418

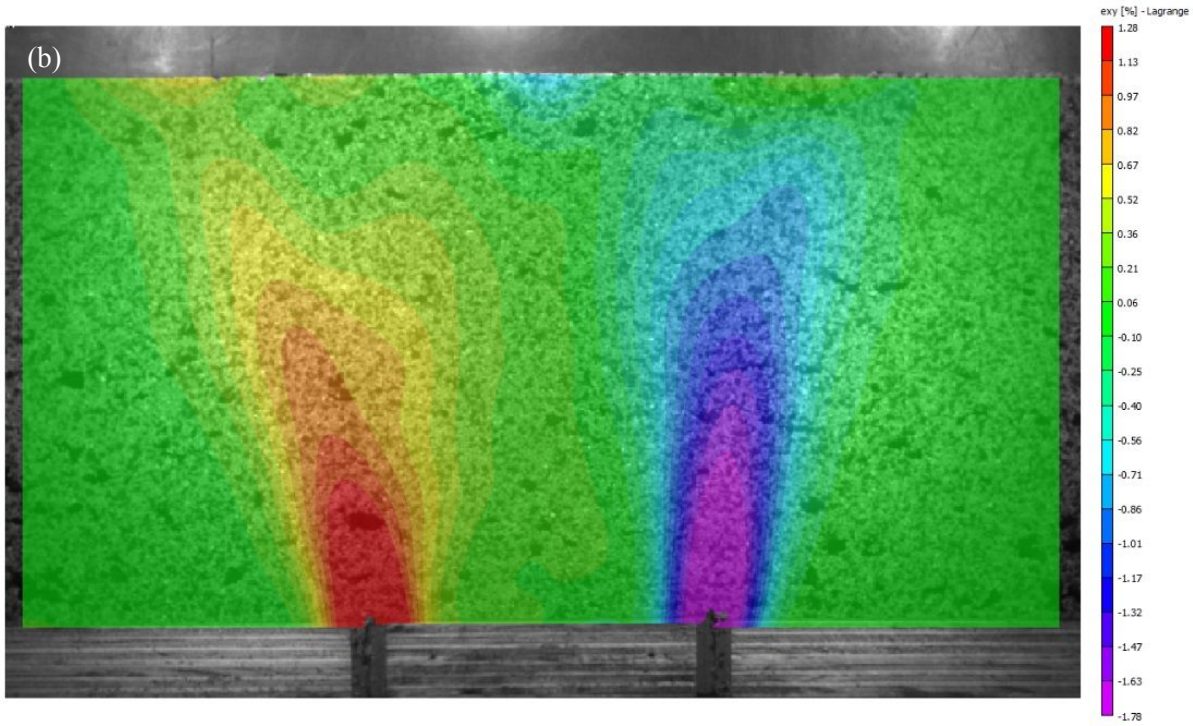

419

420

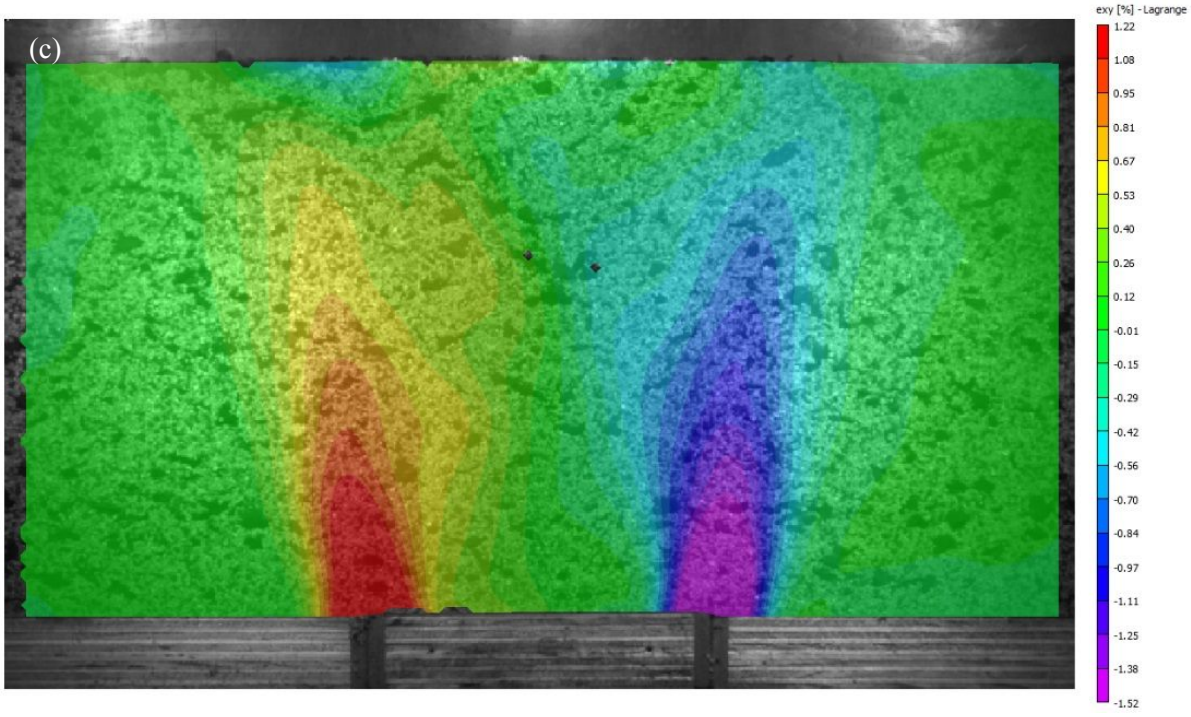

421

422 Fig. 10. Shear strain distribution under no surcharge condition for three materials: (a) Sand,

423 (b) 10% Rubber–sand, and (c) 30% Rubber–sand

424

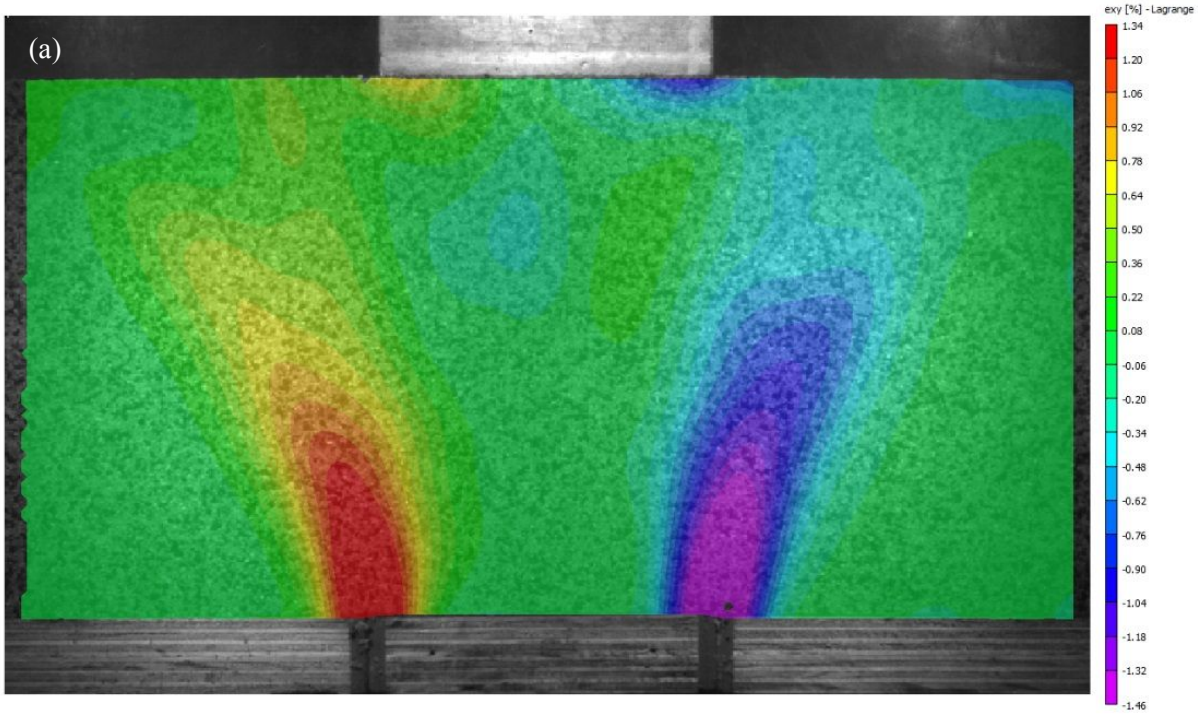

425

426

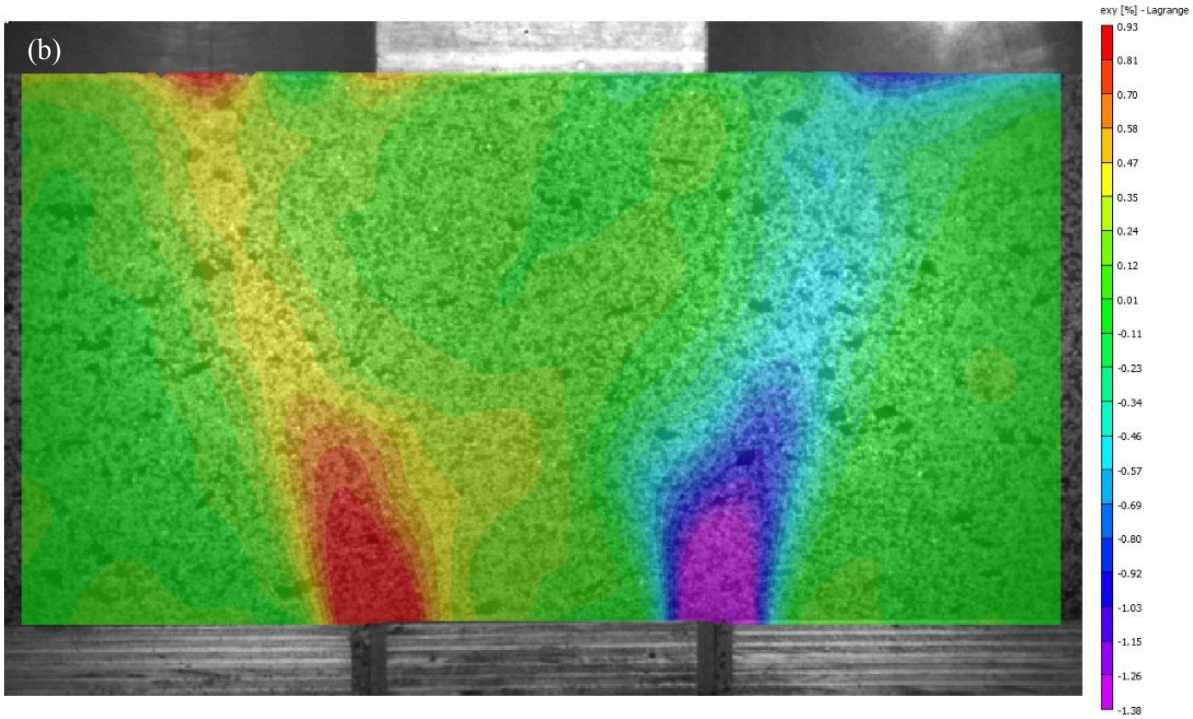

427

428

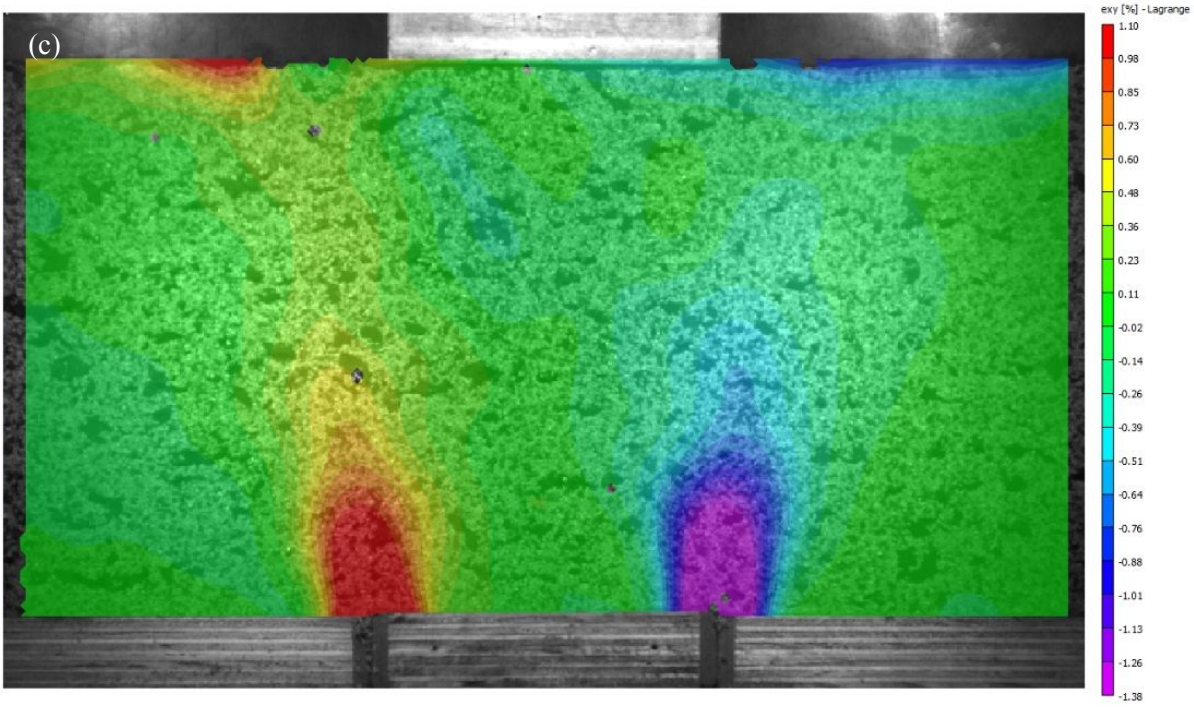

Fig. 11. Shear strain distribution under surcharge loading condition for three materials: (a) Sand, (b) 10% Rubber–sand, and (c) 30% Rubber–sand

As shown in Figs. 10 and 11, in all cases, the shear bands initiated from the trapdoor edges and symmetrically continued in an outward orientation toward the backfill surface. Strain localisation or shear band formation represents the typical deformation behaviour of granular materials under plane-strain conditions (Peters et al., 1988; Alshibli et al., 2003). The shear bands are usually characterised by their angle of inclination and width normalised with respect to particle median size, D_{50}. Table 3 provides the width and inclination angles of the shear bands that evolved in the Sand and rubberised backfills. The angles were measured from the vertical direction and averaged for the two bands. For each band, the width was measured over two profiles in the lower and upper parts of the band, perpendicular to the band axis, where the shear strain values were greater than 50% of the peak shear strain value. As shown in Table 3, regardless of the application of the surcharge, the shear band width

increased minimally with the addition of 10% rubber to the Sand, and then reduced with the further increase in the rubber content to 30%. In the no surcharge case [Fig. 10(a)], the inclination angle of the shear bands decreased with rubber content. The 30% rubber backfill exhibited the lowest inclination angle and the same trend was also observed in the backfills under surcharge loading. The reduction in the inclination angle indicates a shrinkage in the area of the arch. The variation of arching area agrees with the results obtained from the vertical displacement, as presented in Table 2 above.

Table 3. Shear band characteristics under passive arching

Testing conditions	Material	Inclination angle	Dilation angle	Normalised shear band thickness
No surcharge	Sand	12.5°	13°	25.3
	10% Rubber	6.5°	8°	25.9
	30% Rubber	6°	6°	24.2
With surcharge	Sand	13°	8.5°	26.3
	10% Rubber	9.5°	3°	26.7
	30% Rubber	7.5°	5°	22.3

The inclination angle of shear bands in a rising trapdoor is believed to be equal to the angle of dilation of the granular material contained in the apparatus (M.D. Bolton, personal communication, 2018). The angle of dilation is regarded as the characteristic measure of a dilatant material subjected to shearing. On the other hand, negative values of dilation angle will occur in very loose sand with a relative density smaller than 23% (obtained empirically) or dense sand sheared at extremely high normal or confining pressures, where particle

crushing becomes thermodynamically less energy-intensive compared to particle rolling (Bolton 1979, 1986). In these cases, a negative dilation angle indicates contraction during shearing. The amount of plastic volumetric strain developed during plastic shearing is determined by the angle of dilation which is assumed to remain unchanged during plastic yielding. At the idealised critical state, it is naturally inferred that the dilation angle finds a value of zero, hence denoting shearing at constant volume. For natural sand, a dilation angle exceeding 20° is extremely rare (Bolton, 1986). Unlike the friction angle, whose definition remains the same for different modes of shearing (e.g. direct shear test, biaxial or triaxial compression or extension, plane-stain shearing), the expression for the dilation angle depends on the mode of deformation and, therefore, for every case a separate dilation angle is determined mathematically only from plastic strains (Vermeer and de Borst, 1984). By neglecting small elastic strains, for plane-strain conditions, the following expression for the dilation angle (ψ) was proposed by Bolton (1986):

$$\psi = \arcsin\left(-\frac{d\varepsilon_1 + d\varepsilon_2}{d\varepsilon_1 - d\varepsilon_2}\right) \quad (2)$$

where $d\varepsilon_1$ and $d\varepsilon_2$ denote the major and minor principal strain rates. In plasticity theory, the strain rate, denoted here by the letter d preceding the strain ε, are introduced artificially to emphasise an incremental, constitutive response and does not imply a dynamic or rate-related effect (Borja, 2013). The first negative sign is omitted if the tensile strains are considered positive, as is the case in this study. Fig. 12 shows the angle of dilation on a typical Mohr circle of strain, where shear strains are plotted against the normal strains.

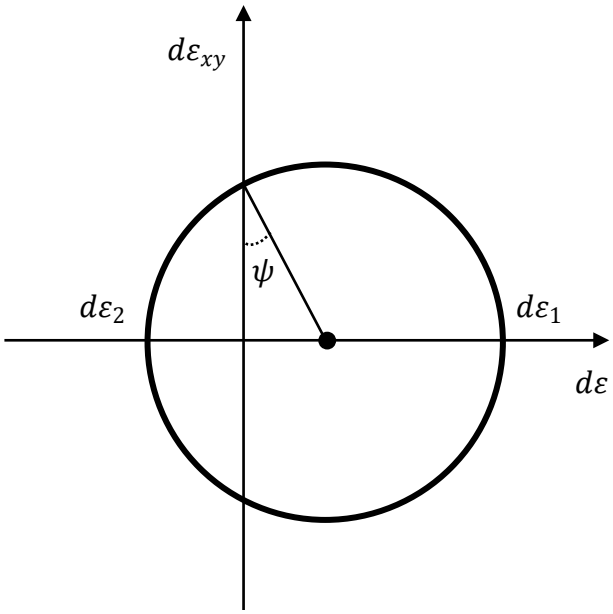

Fig. 12. Mohr circle of strain and the dilation angle for plane-strain conditions

Using the representation in Fig. 12, one can derive the following alternative expression for the angle of dilation under plane-strain conditions in terms of normal and shear strains:

$$\psi = \arcsin\left(\frac{C}{R}\right) \tag{3a}$$

$$C = \frac{d\varepsilon_{xx} + d\varepsilon_{yy}}{2} \tag{3b}$$

$$R = \sqrt{\left(\frac{d\varepsilon_{xx} - d\varepsilon_{yy}}{2}\right)^2 + d\varepsilon_{xy}^2} \tag{3c}$$

where C and R are the x-axis component of the centre point and radius of the Mohr circle of strain, respectively. The average of the horizontal, vertical, and shear strains of two small square elements P_1 and P_2, which are situated inside the shear bands, above the edges of the trapdoor, and have the size of one subset, were extracted from the strain distributions in Figs. 10 and 11 for all the backfills. The corresponding Mohr circles of strain were constructed to obtain the angle of dilation for each shear band. Figs. 13 and 14 show the Mohr circle of

496 strain for the right-hand-side shear bands in the Sand and rubberised backfills. Mohr circles
497 of strain at element P_1, in Fig. 10(a), suggest that the rubber inclusion reduced the
498 deformability of this element. This is reflected in reduced tensile major principal strains. The
499 application of the surcharge resulted in shifting the strains toward one more compressive in
500 nature at this element rather than a tensile one, as shown in Fig. 14. The values of the angle of
501 dilation were then averaged (and rounded to the nearest 0.5°) for each case and are presented
502 in Table 3.

503

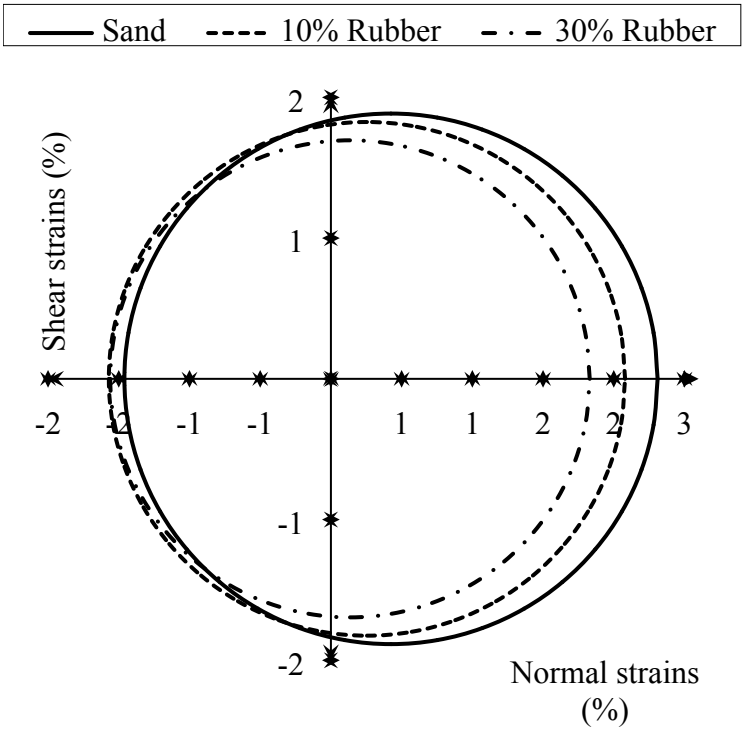

504

505 Fig. 13. Mohr circle of strain for element P_1 in the Sand and Rubber–sand backfills with no
506 surcharge loading

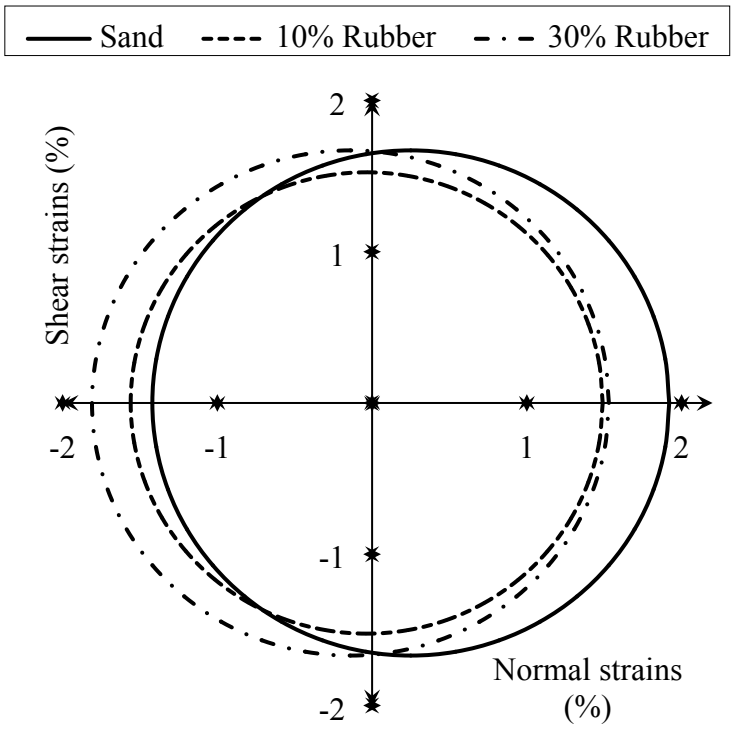

507

508 Fig. 14. Mohr circle of strains for element P_1 in the Sand and Rubber–sand backfills under
509 the application of surcharge

510

511 As shown in Table 3, for the no surcharge cases, excellent agreement is obtained
512 between the angle of dilation of the geomaterials and the angle of inclination of the shear
513 bands. Moderate differences exist between the two sets of values when the surcharge was
514 placed. This reflects the fact that the angle of inclination is dependent on boundary
515 conditions. The local surcharge directed the shear bands to a 'less outward' inclination, where
516 the shear bands became restricted to a rather vertical orientation. Placement of the surcharge
517 block also prevented the growth of the shear bands in the backfills. That is, the shear bands
518 did not evolve upwards, in the surcharge case, to as high an extent as in the no surcharge
519 case. A comparison of the values of the inclination angles of the shear bands with the friction
520 angle (Table 1) and dilation angle (Table 2) suggests that the latter is the more appropriate
521 measure to determine the orientation of the yield surface in the trapdoor apparatus. Use of the

522 friction angle as the inclination angle, on the other hand, more likely leads to erroneous
523 predictions (for example, in the finite element modelling by Wang et al., 2017). In addition to
524 the evidence of direct deformation measurements in this study on the unsuitability of the use
525 of the friction angle, a mathematical sensitivity analysis on the stresses by Singh et al. (2010)
526 showed that soil arching is almost independent of the backfill friction angle.
527

528 **3.4. Stresses**

529 The results of the DIC analysis in the three backfills tested in this study indicated that
530 differential strains were developed in response to the trapdoor displacement. Differential
531 strains in turn result in a redistribution of stresses. The stresses were first recorded on the
532 structure interface for the undeformed Sand and Rubber–sand samples. Verifications were
533 performed on the accuracy of sensors by running trials on at-rest backfills. Excellent
534 agreement was obtained between the theoretical results (based on vertical stress calculations)
535 and the results measured by the sensors. It was observed that, on average, the sensors
536 overestimated the theoretical geostatic stresses by 0.5 kPa for the Sand and by 0.16 kPa for
537 the rubberised backfills. The improved accuracy associated with the rubberised backfills
538 likely arose from the superior adaptation of the rigid sensor surfaces to soft materials, such as
539 the rubber.

540 The stress results of all cases examined in this study are presented in Figs. 15–20. The
541 stress data captured by the sensors, σ_f, were normalised to the initial stress, σ_i, and plotted
542 with respect to trapdoor normalised displacement which is defined as the ratio of trapdoor
543 displacement to the trapdoor width. As can be observed, upon completion of passive arching,
544 the contact stress increased on the trapdoor surface and decreased on the stationary section.

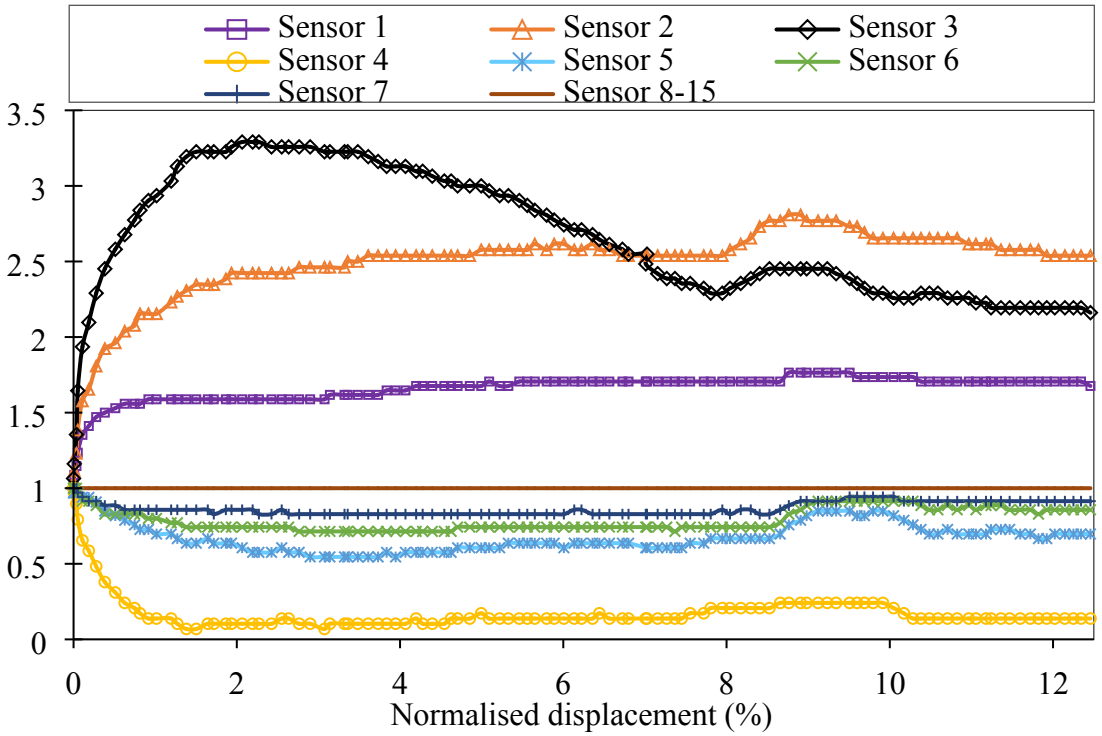

Fig. 15. Measured stress ratios with normalised trapdoor displacement in Sand with no surcharge under passive arching conditions

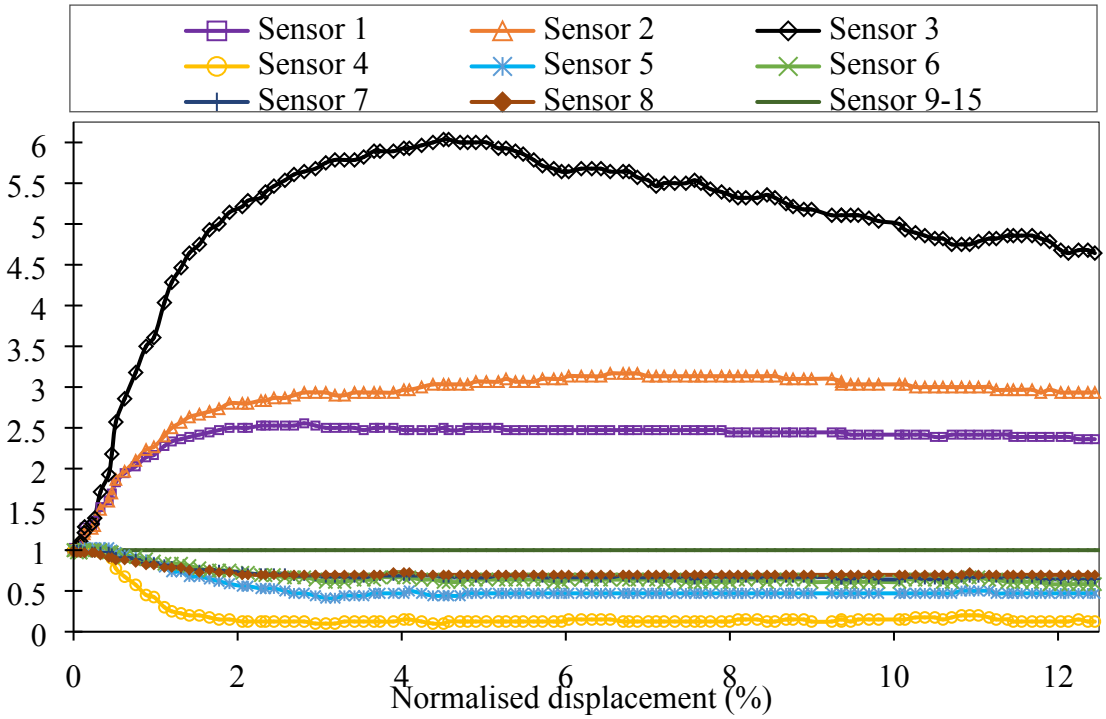

Fig. 16. Measured stress ratios with normalised trapdoor displacement in Sand with a 5 kPa surcharge under passive arching conditions

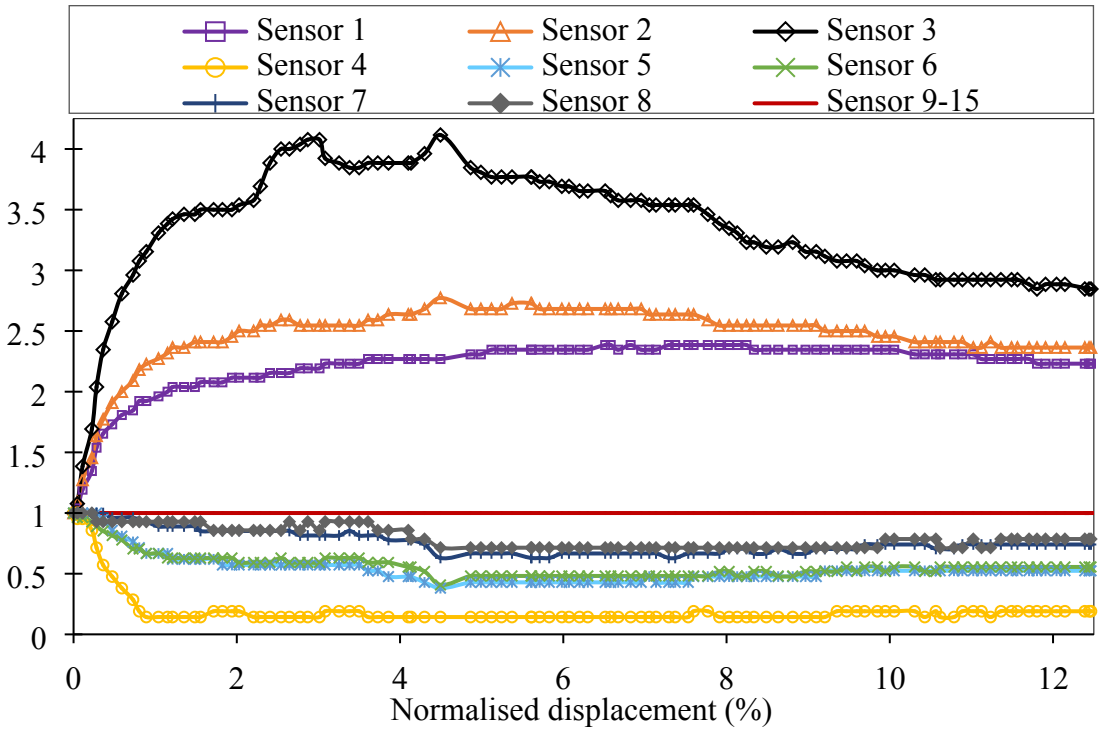

Fig. 17. Measured stress ratios with normalised trapdoor displacement in 10% Rubber–sand with no surcharge under passive arching conditions

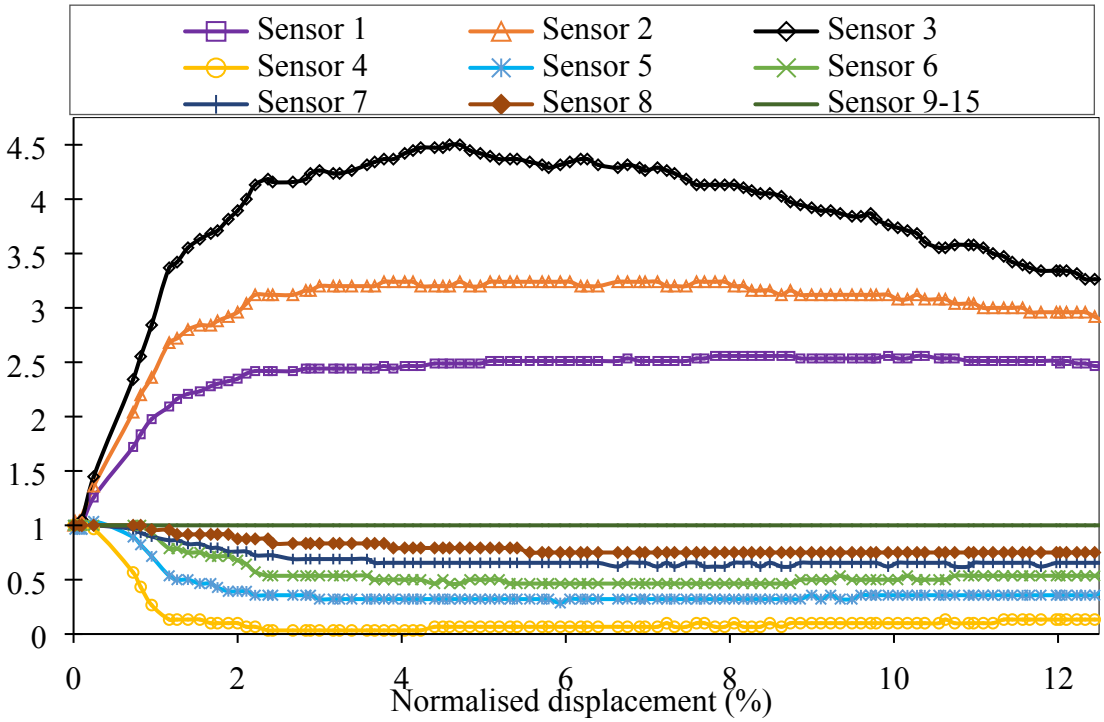

Fig. 18. Measured stress ratios with normalised trapdoor displacement in 10% Rubber–sand with a 5 kPa surcharge under passive arching conditions

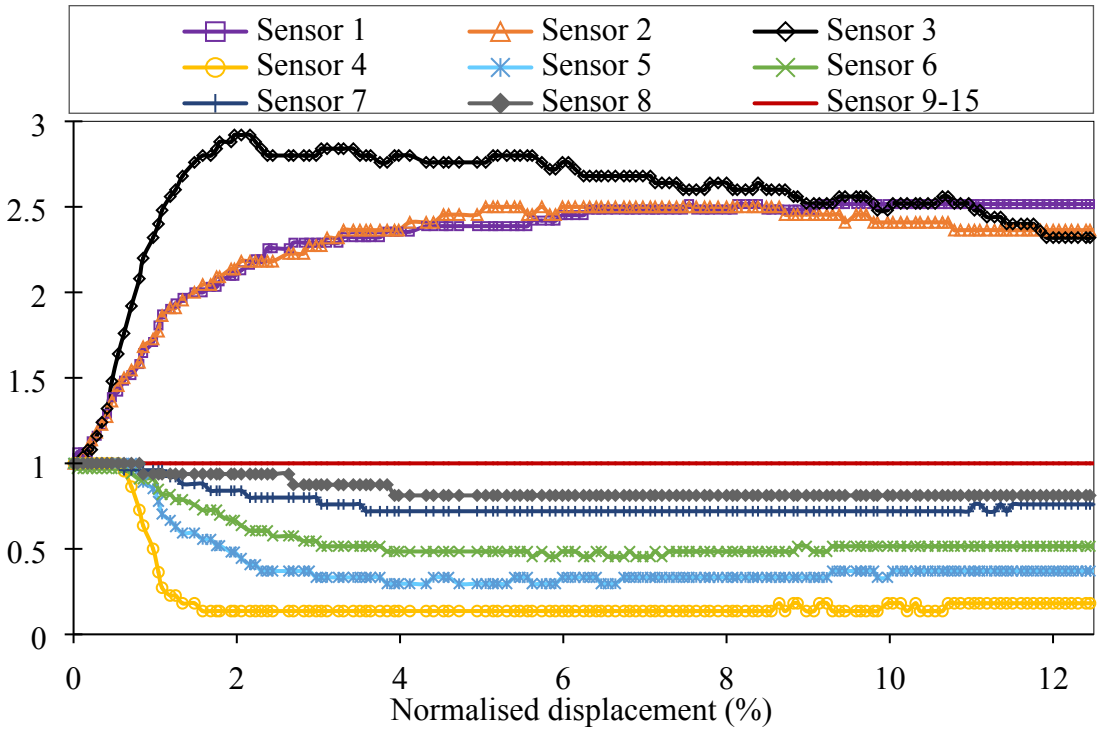

557
558 Fig. 19. Measured stress ratios with normalised trapdoor displacement in 30% Rubber–sand
559 with no surcharge under passive arching conditions

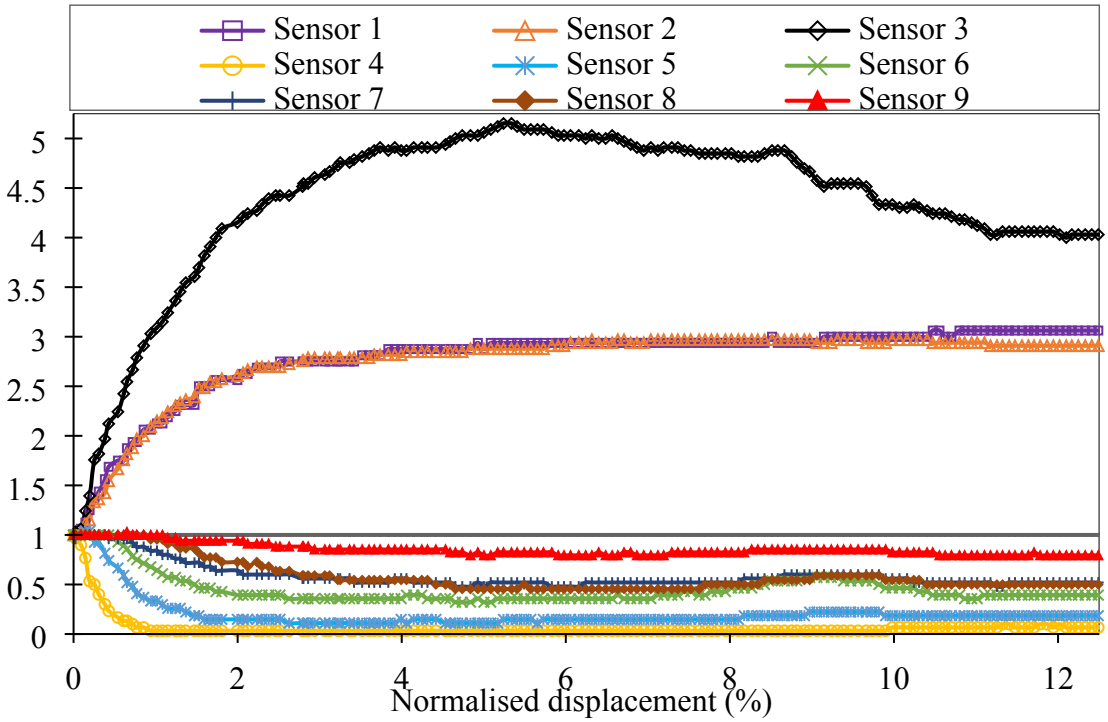

560
561 Fig. 20. Measured stress ratios with normalised trapdoor displacement in 30% Rubber–sand
562 with a 5 kPa surcharge under passive arching conditions

On the trapdoor surface, the stress increase was highest at the trapdoor edge (i.e. Sensor 3), for all cases. At this location, without a surcharge loading, the stresses increased by a factor of 3–4. The factor further increased to 4.5–6 when the surcharge was applied. The stresses for locations distant from the edge (i.e. Sensors 1 and 2) increased by a factor of 1.5–3. The Sand and rubberised backfills exhibited a brittle behaviour along the length that the trapdoor edge sensor represented, i.e. approximately 20% of trapdoor width (TW). However, as the trends, recorded by the trapdoor centre (Sensor 1) and intermediate (Sensor 2) sensors in Figs. 15–20 indicate, the mechanical behaviour of the geomaterials at the interface exhibited a ductile behaviour along the remaining 30% of the trapdoor half-width (recalling that only half of TW was instrumented for stress measurement due to axisymmetry). Therefore, the same geomaterial showed different mechanical behaviours along the length supported by the same structure; that is, brittle behaviour on the outer regions close to the edge of the structure, and ductile behaviour along the internal regions. The least stress change occurred at the trapdoor centre (Sensor 1), in particular, in the cases of Sand and 10% Rubber–sand. Interestingly, very similar stress results were obtained from Sensors 1 and 2 in the 30% Rubber–sand backfill. This similarity in stress values was related to reduced spatial variability and the surcharge loading.

The contact stress distribution depended on at least two factors: the backfill particle size and the surcharge load transferred to the backfill. As the percentage of large rubber particles in the backfills increased, the measurements at the trapdoor centre and intermediate stress sensors gradually became more closely aligned. In other words, the variability in the stress regime decreased. This pattern can be expressed quantitatively if the structure length is normalised with respect to the D_{95} values presented in Table 1 above. The ratios of trapdoor width to the particle size which 95% of the backfill particles are smaller than, are approximately 68, 17, and 14 for the Sand, 10% Rubber–sand, and 30% Rubber–sand

backfills, respectively. Comparing the stress ratio values recorded by the different sensors in Figs. 15–20 with these structure length-to-D_{95} ratios, one concludes that lower spatial variability is observed in the rubberised backfill with the smaller structure length to particle size ratio and higher rubber content. Applying the surcharge also created a similar effect in reducing variability, as reflected in Figs. 15–20. The influence of decreased stress variability due to surcharge loading was extended to the stationary part of the apparatus, as shown by the very close or, on some instances, overlapping sensor readings in this region (e.g. Sensors 7 and 8 in Fig. 20).

On the stationary section of the base of the apparatus, the stress at the interface decreased. The reduction in stress continued until the trapdoor attained to a normalised displacement of 2–3% in all cases, and then the stress remained relatively unchanged with trapdoor displacement, thus exhibiting a ductile response. For all cases, the greatest decrease (of up to 96%) occurred at Sensor 4, which was adjacent to the edge of the stationary section. The influence on stress extended to Sensor 9, in the 30% Rubber–sand with the applied surcharge, and to Sensor 8 in the other cases. This suggests that the passive arching created a zone of influence of 94–113% of the trapdoor width, for the cases examined in this study.

To compare the arching behaviour of Sand and rubberised sand, the concept of tangent arching modulus, first developed by Iglesia et al. (2013) for the active arching mode, is generalised here to the passive arching case at small displacements. A linear relationship between the normalised stress (σ_n) and normalised displacement (ε_n) under passive arching, with an intercept value of unity at zero displacement, can be established from the following expression:

$$\sigma_n = 1 + p_t \cdot \varepsilon_n \quad (4)$$

where p_t denotes the tangent passive arching modulus at small normalised displacements up to 0.5%. The results of ordinary least squares regression, using Eq. (4) for the three backfill materials, are summarised in Table 4. The results are obtained in terms of the stress measured by Sensor 1, and the average stress of Sensors 1–3. As shown in Table 4, the linear relationship fits very well the normalised stress σ_n and normalised displacement ε_n, with a coefficient of determination R^2 of 0.7–1, for most cases examined. Linearity became more pronounced when the stress level in the backfills was increased by the surcharge loading. The Sand showed the highest passive arching modulus among all the backfills tested in this study. Under no surcharge conditions, the arching modulus decreased with increasing rubber content. For example, at the centre of the trapdoor, the modulus decreased by 19% for the 10% Rubber–sand and 66% for the 30% Rubber–sand. These percentages are approximately twice that of the rubber content. When the surcharge was applied, the passive arching moduli reduced in the Sand and 10% Rubber–sand. However, the surcharge loading increased the arching modulus in the 30% Rubber–sand. The reason for this observation is unclear. In the case of 30% Rubber–sand, the moduli increased approximately to the corresponding levels in the Sand. The data in Table 4 indicate that, when a structural element is displaced into sand and rubberised sand backfills (or the backfills move in relation to the structure), as long as the displacements are small, the stress increase at the centre of the jacked structure will be greater in the sand when compared with the rubberised sand backfills.

Table 4. Passive arching moduli in Sand and Rubber–sand mixtures at small normalised displacements

Testing conditions	Material	Measured arching tangent modulus (p_t) on trapdoor			
		Centre	R^2	Average	R^2
No surcharge	Sand	206	0.7	370	0.5
	10% Rubber	167	1	239	0.8
	30% Rubber	69	0.9	71	0.9
With surcharge	Sand	151	1	167	0.9
	10% Rubber	96	1	138	0.9
	30% Rubber	146	1	172	0.7

4. Conclusions

The deformation and stress profiles in Sand, 10% Rubber–sand and 30% Rubber–sand backfills subjected to passive arching in a trapdoor apparatus were presented. The profiles were captured using the DIC technique and a set of stress sensors installed in the apparatus. The following concluding remarks are drawn from the results of the experiments conducted:

- The DIC technique is an effective tool enabling the mapping of deformations in an assembly of granular materials. The technique identified the presence of an arch of equal displacement. In addition, critical zones of straining and local spots of

heterogeneity were observed in the distributions of displacements and strains for a given backfill.

- Rubber inclusions of up to 30% reduced backfill deformation. The 30% Rubber–sand exhibited the lowest shear strains compared to the other two geomaterials, irrespective of the surcharge conditions. The distribution area of vertical displacements was inversely proportional to the rubber content. The addition of rubber to sand marginally influenced the lateral extent of horizontal displacements and strains. Overall, recycled rubber materials can be used to reduce the deformability of the backfills.
- The evolution of shear bands can be predicted by the use of the dilation angle of the materials. The friction angle, on the other hand, is deemed to be unsuitable for the prediction of the shear band evolution. The width and inclination angle of the shear bands were found to be dependent on material type and surcharge conditions.
- Significant increase in stresses on the jacked trapdoor and decrease in the stationary section occurred with the onset of the passive arching. Within the range of small normalised structure displacements (< 0.5%), rubber inclusions helped reduce the arching modulus, thus suggesting a diminished increase in the stresses at the trapdoor. The stress values varied with the measurement location, for all cases. However, in the cases of the rubberised backfills, the difference in stress values between two neighbouring sensors decreased due to the presence of the rubber particles.

Acknowledgements

The first author would like to thank Emeritus Professor Malcom D. Bolton, The University of Cambridge, for his insights on the DIC results presented in the paper. The financial support

673 provided by the University of Adelaide under the Adelaide International Scholarship (ASI)
674 scheme and the Australian Research Council is also acknowledged. The authors wish to thank
675 Mr Gary Bowman for his invaluable assistance in manufacturing the trapdoor apparatus and
676 with the laboratory tests. Special thanks also go to Mr Ian Cates, Mr Thomas Stanef and Mr
677 Simon Golding from the Instrumentation Group of the School of Civil, Environmental and
678 Mining Engineering, and Mr Micah Simonsen from Correlated Solutions, USA, for their
679 valuable technical advice and assistance.

680

681 **References**

682 ASTM, 2017. Standard practice for use of scrap tires in civil engineering applications
683 ASTM D6270 – 17, ASTM International, West Conshohocken, PA, USA.
684 ASTM, 2018. Standard test method for measurement of hydraulic conductivity of materials
685 derived from scrap tires using a rigid wall permeameter ASTM D7760 – 18, ASTM
686 International, West Conshohocken, PA, USA.
687 Ahn, I.S., and Cheng, L. 2014. Tyre derived aggregate for retaining wall backfill under
688 earthquake loading. Construction and Building Materials, **57**: 105–116.
689 Alshibli, K.A., Batiste, S.N., and Sture, S. 2003. Strain localization in sand: Plane strain
690 versus triaxial compression. Journal of Geotechnical and Geoenvironmental
691 Engineering, **129**(6): 483–494.
692 Aqoub, K., Mohamed, M., and Sheehan, T. 2018. Analysis of sequential active and passive
693 arching in granular soils, International Journal of Geotechnical Engineering DOI:
694 10.1080/19386362.2018.1473195.
695 Bolton, M.D. 1979. A guide to soil mechanics. Macmillan, London.
696 Bolton, M.D. 1986. The strength and dilatancy of sands. Geotechnique, **36**(1): 65–78.

Borja, R. 2013. Plasticity: Modelling and computation (Chapter 1). Springer, Berlin.

Bosscher, P.J., Edil, T.B., and Kuraoka, S. 1997. Design of highway embankments using tyre chips. Journal of Geotechnical and Geoenvironmental Engineering, **123**(4): 295–304.

Chen, C.-Y., and Martin, G.R. 2002. Soil–structure interaction for landslide stabilizing piles. Computers and Geotechnics, **29**(5): 363–386.

Chevalier, B., Combe, G., and Villard, P. 2012. Experimental and discrete element modeling studies of the trapdoor problem: Influence of the macro-mechanical frictional parameters. Acta Geotechnia, **7**(1): 15–39.

Costa, Y.D., Zornberg, J.G., Bueno, B.S., and Costa, C.L. 2009. Failure mechanisms in sand over a deep active trapdoor. Journal of Geotechnical and Geoenvironmental Engineering, **135**(11): 1741–1753.

Dewoolkar, M.M., Santichaianant, K., and Ko, H.Y. 2007. Centrifuge modelling of granular soil response over active circular trapdoors. Soils and Foundations, **47**(5): 931–945.

Edil, T., and Bosscher, P. 1994. Engineering properties of tyre chips and soil mixtures. Geotechnical Testing Journal, **17** (4): 453–464.

Edil, T.B. 2004. A review of mechanical and chemical properties of shredded tyres and soil mixtures. Recycled Materials in Geotechnics, American Society of Civil Engineers, GSP127, A.H. Aydilek and J. Wartman, eds., ASCE Baltimore, pp.1–21.

Edinçliler, A., Baykal G., and Dengili, K. 2004. Determination of static and dynamic behaviour of recycled materials for highways. Resources, Conservation and Recycling, **42**: 23–237.

Eldin, N.N., and Senouti, A.B. 1992. Use of scrap tyre in road construction. Journal of Construction Engineering and Management, **118**: 561–576.

He, Y., Hazarika, H., Yasufuku, N., and Han, Z. 2015. Evaluating the effect of slope angle on the distribution of the soil–pile pressure acting on stabilizing piles in sandy slopes. Computers and Geotechnics, **69**: 153–165.

Head, K., and Epps, R.J. 2010. Manual of soil laboratory testing: Permeability, shear strength and compressibility tests (Volume 2, Chapter 12), 3rd edition, Whittles Publishing.

Humphery, D.N., and Sandford, T.C. 1993. Tyre chips as lightweight subgrade fill and retaining wall backfill. Proceedings of the Symposium on Recovery and Effective reuse of Discarded Materials and By-Products for Construction of Highway Facilities, Federal Highway Administration, Washington, D.C.

Humphrey, D.N. 1999. Civil engineering applications of chipped tyres. Research Report, North Platte, Nebraska.

Humphrey, D.N., and Blumenthal, M. 2010. The use of tyre-derived aggregate in road construction applications. Green Streets and Highways 2010: An interactive Conference on the State of the Art and How to Achieve Sustainable Outcomes. Weinstein, N., ed., Reston, VA, USA: American Society of Civil Engineers, 2010.

Iglesia, G.R., Einstein, H.H., and Whitman, R.V. 2013. Investigation of soil arching with centrifuge tests. Journal of Geotechnical and Geoenvironmental Engineering, **140**(2): 04013005.

Kahyaoğlu, M.R., Onal, O., Imançlı, G., Ozden G., and Kayalar, A.Ş. 2012. Soil arching and load transfer mechanism for slope stabilized with piles, Journal of Civil Engineering and Management, **18**(5): 701–708.

Khatami, H., Deng, A., Jaksa, M. 2019. An experimental study of the active arching effect in soil using the digital image correlation technique. Computers and Geotechnics **108**: 183–196.

747 Lee, H.J., and Roh, H.S. 2007. The use of recycled tyre chips to minimize dynamic earth
748 pressure during compaction of backfill. Construction and Building Materials, **21**:
749 1016–1026.
750 Lee, J.H., Salgado, R., Bernal, A., and Lovell, C.W. 1999. Shredded tyres and rubber-sand
751 as lightweight backfill. Journal of Geotechnical and Geoenvironmental Engineering,
752 **125** (2): 132–141.
753 Look, B. (2007). Handbook of geotechnical investigation and design tables. Taylor &
754 Francis Group, London, UK.
755 Mair, R.J. (1979). Centrifugal modelling of tunnel construction in soft clay. PhD thesis,
756 Cambridge University, UK.
757 Pan, B., Xie, H., Wang, Z., Qian, K., and Wang, Z. 2008. Study on subset size selection in
758 digital image correlation for speckle patterns. Optic Express, **16**(10): 7037–7048.
759 Peters, J., Lade, P., and Bro, A. 1988. Shear band formation in triaxial and plane strain
760 tests. Advanced triaxial testing of soil and rock, ASTM, STP 977, R. Donaghe, R.
761 Chaney, and M. Silver, eds., ASTM, 604–627.
762 Rubber Manufacturers Association (RMA), 2013. U.S. Scrap tyre market summary in
763 2011.
764 Schreier, H., Orteu, J., and Sutton, M. 2009. Image correlation for shape, motion and
765 deformation measurements. Boston, MA: Springer US.
766 Shalaby, A., and Khan, R.A. 2005. Design of unsurfaced roads constructed with large-size
767 shredded rubber tyres: a case study. Resources, Conservation and Recycling, **44**: 318–
768 332.
769 Shelke, A., and Patra, N.R. 2008. Effect of arching on uplift capacity of pile groups in sand.
770 International Journal of Geomechanics, **8**(6): 347–354.

Singh, S., Sivakugan, N., and Shukla, S. 2010. Can soil arching be insensitive to φ? International Journal of Geomechanics, **10**(3): 124–128.

Standards Australia, 1998. Australian Standard AS 1289.5.5.1 Soil compaction and density tests – Determination of the minimum and maximum dry density of a cohesionless material – Standard method.

Standards Australia, 1998. Australian Standard AS 1289.6.2.2 Methods of testing soils for engineering purposes – Soil strength and consolidation tests – Determination of shear strength of a soil – Direct shear test using a shear box.

Talesnick, M. 2013. Measuring soil pressure within a soil mass. Canadian Geotechnical Journal, **50**(7): 716-722

Terzaghi, K. 1936. Stress distribution in dry and in saturated sand above a yielding trap-door. Proceedings of the International Conference on Soil Mechanics and Foundation Engineering, Vol. I, pp. 307–311.

Tweedie, J.J., Humphrey, D.N., and Sandford, T.C. 1998. Full scale field trials of tyre shreds as lightweight retaining wall backfill, at-test condition. Preprint, Transportation Research Board, Washington, D.C.

Tyrecycle, 2018. http://www.tyrecycle.com.au. Accessed 20/09/18.

van Eekelen, S.J.M. 2015. Basal reinforced piled embankments: Experiments, field studies and the development and validation of a new analytical design model. PhD thesis, Department of Geoscience and Engineering, Delft University of Technology.

Vermeer, P.A., and de Borst, R. 1998. Non-associated plasticity for soils, concrete and rock. HERON, **29**(3): 1984.29.

Wang, L., Leshchinsky, Evans, T.M., and Xie, Y. 2017. Active and passive arching stresses in c′-ϕ′ soils: A sensitivity study using computational limit analysis. Computers and Geotechnics, **84**: 47–57.

796 Yoon, S., Prezzi, M., Siddiki, N.Z., and Kim, B. 2006. Construction of a test embankment
797 using a sand-tyre shred mixture as fill material. Waste Management, **26**(9): 1033–
798 1044.
799 Yuan, B., Chen, R., Teng, J., Peng, T., and Feng, Z. 2014. Effect of passive pile on 3D
800 ground deformation and on active pile response. The Scientific World Journal, 2014:
801 904186.

802
803
804
805
806

807 **Tables captions**

808

809 Table 1. Physical properties of the backfill materials

810 Table 2. Area of arch and crest height of the arch of equal displacement in different backfills

811 Table 3. Shear band characteristics under passive arching

812
813
814
815
816
817
818

819

820

821

822

823

824

825

826 **Figures captions**

827 Fig. 1. The instrumented trapdoor apparatus: (a) stress sensor array, (b) imaging equipment

828 Fig. 2. Distribution of horizontal displacements under no-surcharge conditions for the three
829 materials: (a) Sand, (b) 10% Rubber–sand, and (c) 30% Rubber–sand

830 Fig. 3. Distribution of horizontal displacements with the application of the 5 kPa surcharge
831 for the three materials: (a) Sand, (b) 10% Rubber–sand, and (c) 30% Rubber–sand

832 Fig. 4. Horizontal strain distributions under no surcharge conditions for the three materials:
833 (a) Sand, (b) 10% Rubber–sand, and (c) 30% Rubber–sand

834 Fig. 5. Horizontal strain distributions with the application of surcharge for the three materials:
835 (a) Sand, (b) 10% Rubber–sand, and (c) 30% Rubber–sand

836 Fig. 6. Distributions of vertical displacements under no surcharge conditions for the three
837 materials: (a) Sand, (b) 10% Rubber–sand, and (c) 30% Rubber–sand

838 Fig. 7. Distributions of vertical displacements with the application of surcharge for the three
839 materials: (a) Sand, (b) 10% Rubber–sand, and (c) 30% Rubber–sand

840 Fig. 8. Vertical strain distributions under no surcharge for the three materials: (a) Sand, (b)
841 10% Rubber–sand, and (c) 30% Rubber–sand

842 Fig. 9. Vertical strain distributions with the application of surcharge for the three materials:
843 (a) Sand, (b) 10% Rubber–sand, and (c) 30% Rubber–sand

844 Fig. 10. Shear strain distribution under no surcharge condition for three materials: (a) Sand,
845 (b) 10% Rubber–sand, and (c) 30% Rubber–sand

846 Fig. 11. Shear strain distribution under surcharge loading condition for three materials: (a)
847 Sand, (b) 10% Rubber–sand, and (c) 30% Rubber–sand

848 Fig. 12. Mohr circle of strain and the dilation angle for plane-strain conditions

849 Fig. 13. Mohr circle of strain for element P1 in the Sand and Rubber–sand backfills with no
850 surcharge loading

851 Fig. 14. Mohr circle of strains for element P1 in the Sand and Rubber–sand backfills under
852 the application of surcharge

853 Fig. 15. Measured stress ratios with normalised trapdoor displacement in Sand with no
854 surcharge under passive arching conditions

855 Fig. 16. Measured stress ratios with normalised trapdoor displacement in Sand with a 5 kPa
856 surcharge under passive arching conditions

857 Fig. 17. Measured stress ratios with normalised trapdoor displacement in 10% Rubber–sand
858 with no surcharge under passive arching conditions

859 Fig. 18. Measured stress ratios with normalised trapdoor displacement in 10% Rubber–sand
860 with a 5 kPa surcharge under passive arching conditions

861 Fig. 19. Measured stress ratios with normalised trapdoor displacement in 30% Rubber–sand
862 with no surcharge under passive arching conditions

863 Fig. 20. Measured stress ratios with normalised trapdoor displacement in 30% Rubber–sand
864 with a 5 kPa surcharge under passive arching conditions